

**PYRROLIDINE AS A PROMOTER FOR METHANE HYDRATE  
FORMATION: COMPARATIVE STUDY ON THE THERMODYNAMICS,  
KINETICS, AND MORPHOLOGY WITH TETRAHYDROFURAN**

Siravich Junthong

A Thesis Submitted in Partial Fulfillment of the Requirements  
for the Degree of Master of Science  
The Petroleum and Petrochemical College, Chulalongkorn University  
in Academic Partnership with  
The University of Michigan, The University of Oklahoma,  
and Case Western Reserve University

2021



3243175980

3243175980  
CD IThesis 6271006063 thesis / recv: 19072564 14:31:51 / seq: 40

# Pyrrolidine as a Promoter for Methane Hydrate Formation: Comparative Study on the Thermodynamics, Kinetics, and Morphology with Tetrahydrofuran

Mr. Siravich Junthong

A Thesis Submitted in Partial Fulfillment of the Requirements  
for the Degree of Master of Science in Petrochemical Technology  
Common Course  
The Petroleum and Petrochemical College  
Chulalongkorn University  
Academic Year 2020  
Copyright of Chulalongkorn University



3243175980

CU ThesIs 6271006063 thesis / recv: 19072564 14:31:51 / seq: 40

โปโลลิคินในฐานะตัวเร่งสำหรับการเกิดมีเทนไฮเดรต: การศึกษาเชิงเปรียบเทียบในมิติของอุณหภูมิ  
หพลศาสตร์ จลนพลศาสตร์ และสัณฐานวิทยากับเตตระไฮโดรฟิวแรน

นายสิริวิชญ์ จันท์ทอง

วิทยานิพนธ์นี้เป็นส่วนหนึ่งของการศึกษาตามหลักสูตรปริญญาวิทยาศาสตรมหาบัณฑิต  
สาขาวิชาเทคโนโลยีปิโตรเคมี ไม่สังกัดภาควิชา/...  
วิทยาลัยปิโตรเลียมและปิโตรเคมี จุฬาลงกรณ์มหาวิทยาลัย  
ปีการศึกษา 2563  
ลิขสิทธิ์ของจุฬาลงกรณ์มหาวิทยาลัย



3243175980

CU Thesisis 6271006063 thesis / recv: 19072564 14:31:51 / seq: 40

Thesis Title                      Pyrrolidine as a Promoter for Methane Hydrate  
Formation: Comparative Study on the Thermodynamics,  
Kinetics, and Morphology with Tetrahydrofuran  
By                                      Mr. Siravich Junthong  
Field of Study                      Petrochemical Technology  
Thesis Advisor                      Professor PRAMOCH RANGSUNVIGIT, Ph.D.  
Thesis Co Advisor                      Santi Kulprathipanja, Ph.D.

---

Accepted by The Petroleum and Petrochemical College, Chulalongkorn University  
in Partial Fulfillment of the Requirement for the Master of Science

..... Dean of The Petroleum and  
Petrochemical College  
(Professor PRAMOCH RANGSUNVIGIT, Ph.D.)

#### THESIS COMMITTEE

..... Chairman  
(Assistant Professor UTHAIORN  
SURIYAPRAPHADILOK, Ph.D.)  
..... Thesis Advisor  
(Professor PRAMOCH RANGSUNVIGIT, Ph.D.)  
..... Thesis Co-Advisor  
(Santi Kulprathipanja, Ph.D.)  
..... External Examiner  
(Tanate Danuthai, Ph.D.)



3243175980

CD IThesis 6271006063 thesis / recv: 19072564 14:31:51 / seq: 40

สิริวิชญ์ จันทรทอง : ไพโรลิดีนในฐานะตัวเร่งสำหรับการเกิดมีเทนไฮเดรต: การศึกษาเชิงเปรียบเทียบ  
 ในมิติของอุณหพลศาสตร์ จลนพลศาสตร์ และสัณฐานวิทยาเกี่ยวกับเตตระไฮโดรฟูแรน. (Pyrrolidine as a  
 Promoter for Methane Hydrate Formation: Comparative Study on the Thermodynamics, Kinetics, and  
 Morphology with Tetrahydrofuran) อ.ที่ปรึกษาหลัก : ศ. ดร.ปราโมช รั้งสรรค์วิจิตร, อ.ที่ปรึกษาร่วม :  
 ดร.สันติ กุลประทีปปัญญา

แก๊สธรรมชาติในรูปแบบของแข็ง (SNG) โดยเทคโนโลยีไฮเดรตได้รับการเสนอให้เป็นเทคโนโลยี  
 ทางเลือกสำหรับการกักเก็บและการขนส่งแก๊สธรรมชาติอันเนื่องมาจากมีข้อดีหลายประการ อย่างไรก็ตาม  
 อัตราการเกิดไฮเดรตที่ช้าและความต้องการสภาวะการทำงานที่รุนแรงยังคงเป็นข้อจำกัดสำคัญที่ต้องปรับปรุง  
 เพื่อให้เทคโนโลยีดังกล่าวสามารถแข่งขันและนำไปประยุกต์ใช้ในเชิงอุตสาหกรรมได้ งานวิจัยนี้จึงศึกษาบทบาท  
 ของไพโรลิดีน (Pyrrolidine) ที่ความเข้มข้นร้อยละ 5.56 โดยโมลในมิติของอุณหพลศาสตร์ จลนพลศาสตร์ และ  
 สัณฐานวิทยาที่มีต่อการเกิดมีเทนไฮเดรต ผลการศึกษาพบว่าไพโรลิดีนสามารถช่วยเพิ่มเสถียรภาพเชิงอุณหพล  
 ศาสตร์ของมีเทนไฮเดรตได้ โดยทำให้การเกิดมีเทนไฮเดรตนั้นเกิดขึ้นในสภาวะรุนแรงน้อยลงเมื่อเปรียบเทียบกับ  
 สภาวะการเกิดของมีเทนไฮเดรตบริสุทธิ์ ในมิติของประสิทธิภาพเชิงจลศาสตร์ การทดลองดำเนินการที่ความดัน  
 8 เมกะพาสคาลและอุณหภูมิ 285.2 เคลวิน ผลการวิจัยพบว่าไพโรลิดีนสามารถลดระยะเวลาในการเหนี่ยวนำ  
 การเกิดไฮเดรต รวมถึงเร่งอัตราการเกิดไฮเดรตควบคู่ไปกับความสามารถในการกักเก็บแก๊สมีเทนที่น่าพอใจ  
 สำหรับการทดลองเชิงสัณฐานวิทยา ฟองมีเทนซึ่งถือเป็นลักษณะสำคัญถูกค้นพบระหว่างการเกิดมีเทนไฮเดรต  
 ซึ่งลักษณะสำคัญนี้มีผลอย่างยิ่งในการช่วยให้แก๊สมีเทนสามารถทำปฏิกิริยากับสารละลายได้มากขึ้น นอกจากนี้  
 ยังได้ศึกษาเชิงจลนพลศาสตร์เพื่อเปรียบเทียบกับเตตระไฮโดรฟูแรน (THF) ภายใต้แรงขับเคลื่อนเดียวกันและ  
 ภายใต้สภาวะเดียวกัน ผลการศึกษาพบว่าถึงแม้เตตระไฮโดรฟูแรนสามารถกักเก็บแก๊สมากกว่า แต่ไพโรลิดีนให้  
 อัตราการเกิดไฮเดรตสูงกว่า 10 เท่าเมื่อเปรียบเทียบกับภายใต้แรงขับเคลื่อนเดียวกัน และยังให้อัตราการเกิดไฮเดรตที่  
 เทียบเคียงกับเตตระไฮโดรฟูแรนภายใต้สภาวะเดียวกัน การค้นพบในการวิจัยนี้สามารถใช้เป็นข้อมูลพื้นฐาน  
 และข้อมูลเชิงลึกที่เป็นประโยชน์ในการเลือกใช้ตัวเร่งการเกิดไฮเดรตที่เหมาะสมสำหรับเทคโนโลยีการกักเก็บ  
 แก๊สธรรมชาติในรูปแบบของแข็งในเชิงพาณิชย์

สาขาวิชา	เทคโนโลยีปิโตรเคมี	ลายมือชื่อนิสิต .....
ปีการศึกษา	2563	ลายมือชื่อ อ.ที่ปรึกษาหลัก ..... ลายมือชื่อ อ.ที่ปรึกษาร่วม .....

# # 6271006063 : MAJOR PETROCHEMICAL TECHNOLOGY

KEYWOR Methane hydrate formation, Phase equilibrium, Pyrrolidine,  
D: Tetrahydrofuran

Siravich Junthong : Pyrrolidine as a Promoter for Methane Hydrate Formation: Comparative Study on the Thermodynamics, Kinetics, and Morphology with Tetrahydrofuran. Advisor: Prof. PRAMOCH RANGSUNVIGIT, Ph.D. Co-advisor: Santi Kulprathipanja, Ph.D.

Solidified natural gas (SNG) via clathrate hydrates has been proposed as an alternative approach for natural gas storage and transportation due to its numerous advantages. However, a slow hydrate formation rate and a requirement of operating conditions are the major limitations, which need to be improved to make SNG competitive in a large scale deployment. In this work, the roles of 5.56 mol% pyrrolidine were investigated for the methane hydrate formation in terms of thermodynamics and kinetics along with morphology. The results showed that pyrrolidine generally improved the thermodynamic stability of mixed methane hydrates, enhancing the formation at milder conditions than those of pure methane hydrates. To demonstrate the kinetic performance of pyrrolidine, the experiments were performed at 8 MPa and 285.2 K in a quiescent configuration. The results showed that a very short induction time and a rapid rate of hydrate formation with desirable methane uptake were achieved. In addition, a distinct methane bubble with breathing effect, assisting methane gas to interact with the bulk solution, was observed during the hydrate formation morphology. The comparative kinetic study with 5.56 mol% THF was also carried out under the same driving force and the same experimental condition. Surprisingly, although THF gave a high methane uptake, pyrrolidine could give more than 10 times higher rate of hydrate formation at the same driving force; moreover, it provided a competitive rate with THF at the similar formation condition. These findings may provide the fundamental backgrounds and give a useful insight to select the appropriate hydrate promoter for the clathrate hydrates and the commercialized SNG technology.

Field of Study:	Petrochemical Technology	Student's Signature
		.....
Academic	2020	Advisor's Signature
Year:		.....
		Co-advisor's Signature
		.....

## ACKNOWLEDGEMENTS

I would like to take this opportunity to express my deep special thanks to my thesis advisor, Prof. Pramoch Rangsunvigit, who gives me a chance to prepare this research. He also provides me an elevating inspiration and supports me to conquer every problem. His suggestion, discussion, and supervision from the beginning throughout my thesis are very helpful and motivate me to overcome the limitations.

I would like to offer my sincere thanks to my co-advisor, Dr. Santi Kulprathipanja, for his advice and guidance. His bright thoughts can ignite me many ideas to further develop my research.

My sincere thanks also go Asst. Prof. Uthaiporn Suriyapraphadilok and Dr. Tanate Danuthai for kindly serving on my thesis committee. Their comments and suggestions are also necessary for the completion of my thesis.

I am particularly grateful for the full scholarship provided by Bangchak Corporation Public Company Limited on the occasion of the 30th Anniversary of The Petroleum and Petrochemical College, Chulalongkorn University.

I feel to acknowledge the assistance from Miss Viphada Yodpetch, Mr. Katipot Inkong, Mr. Chakorn Virirakul, and Mr. Kan Jeenmuang for their advice and being my best companion.

Finally, I would like to thank the entire faculty and staff at The Petroleum and Petrochemical College, Chulalongkorn University for their kind assistance and cooperation.

Siravich Junthong

# TABLE OF CONTENTS

	<b>Page</b>
ABSTRACT (THAI) .....	iii
ABSTRACT (ENGLISH).....	iv
ACKNOWLEDGEMENTS .....	v
TABLE OF CONTENTS.....	vi
LIST OF TABLES .....	ix
LIST OF FIGURES .....	x
CHAPTER 1 INTRODUCTION .....	1
CHAPTER 2 LITERATURE REVIEW .....	4
2.1 Natural Gas .....	4
2.2 Natural Gas Storage and Transportation.....	5
2.2.1 Compressed Natural Gas (CNG).....	5
2.2.2 Liquefied Natural Gas (LNG) .....	6
2.2.3 Adsorbed Natural Gas (ANG).....	6
2.3 Gas Hydrates.....	7
2.3.1 Early History .....	7
2.3.2 Definition.....	8
2.3.3 Structure and Characteristics of Hydrates .....	9
2.3.3.1 Structure I (sI) .....	10
2.3.3.2 Structure II (sII).....	10
2.3.3.3 Structure H (sH) .....	11
2.3.4 Clathrate Hydrates .....	11
2.4 Hydrate Formation.....	12
2.4.1 Hydrate Nucleation.....	12
2.4.2 Hydrate Growth.....	13
2.5 Hydrate Dissociation .....	14



2.6 Hydrate Promoter.....	15
2.6.1 Kinetic Promoter .....	15
2.6.1.1 Surfactants .....	15
2.6.1.2 Amino Acids.....	18
2.6.2 Thermodynamic Promoter.....	21
2.6.2.1 Tetrahydrofuran (THF).....	21
2.6.2.2 Pyrrolidine .....	25
CHAPTER 3 EXPERIMENTAL.....	26
3.1 Materials and Equipment .....	26
3.1.1 Chemicals .....	26
3.1.2 Hydrate Formation / Dissociation Apparatus.....	26
3.2 Experiment Procedures .....	27
3.2.1 Experiment Apparatus .....	27
3.2.2 Experiment Procedure for Thermodynamic Studies .....	28
3.2.3 Experiment Procedure for Kinetic and Morphology Studies .....	29
CHAPTER 4 RESULTS AND DISCUSSION.....	32
4.1 Thermodynamic Study: Phase Equilibrium Measurement for Methane- pyrrolidine and Methane-THF Hydrate System .....	32
4.2 Kinetic and Morphology Studies .....	38
4.2.1 Mixed Methane-pyrrolidine Hydrate Formation under Moderate Condition .....	38
4.2.2 Effects of the Same Driving Force and the Same Experimental Condition on the Mixed Methane-pyrrolidine and Mixed Methane-THF Hydrate Formation .....	45
4.2.3 Mixed Methane-THF and Mixed Methane-pyrrolidine Hydrate Dissociation .....	52
CHAPTER 5 CONCLUSIONS AND RECCOMENDATIONS.....	55
5.1 Conclusions.....	55
5.2 Recommendations.....	55
APPENDICES .....	57
Appendix A Graphical Abstract .....	57

Appendix B Supporting Information .....58  
REFERENCES .....60  
VITA.....67



3243175980

CU IThesis 6271006063 thesis / recv: 19072564 14:31:51 / seq: 40

## LIST OF TABLES

	<b>Page</b>
<b>Table 2.1</b> History timeline of methane gas hydrates .....	7
<b>Table 2.2</b> Characteristics of three hydrate structures .....	10
<b>Table 2.3</b> Average data for results of hydrate formation for experiments conducted at 7.2 MPa and different temperatures .....	22
<b>Table 4.1</b> Equilibrium data obtained in this study for the mixed methane-pyrrolidine hydrate and methane-THF hydrate systems.....	33
<b>Table 4.2</b> Summary of the experimental results for the methane hydrate formation of 5.56 mol% promoters at both same driving force and same experimental condition..	39

## LIST OF FIGURES

	Page
<b>Figure 2.1</b> Natural gas formation .....	4
<b>Figure 2.2</b> Natural gas storage and transportation .....	5
<b>Figure 2.3</b> Methane hydrate pellet samples .....	8
<b>Figure 2.4</b> Three common structure of hydrates: sI, sII and sH.....	9
<b>Figure 2.5</b> Schematic view of clathrate hydrate structure.....	11
<b>Figure 2.6</b> Conceptual of hydrate nucleation .....	12
<b>Figure 2.7</b> Conceptual model of hydrate growth process: mass transfer, diffusion of gas into stagnant layer and the incorporation into hydrate .....	13
<b>Figure 2.8</b> Three common methods for the hydrate dissociation.....	14
<b>Figure 2.9</b> Methane hydrate formation rate at different concentrations of SDS, an anionic surfactant .....	15
<b>Figure 2.10</b> Methane hydrate formation rate at different concentrations of LABS, an anionic surfactant .....	16
<b>Figure 2.11</b> Methane hydrate formation rate at different concentrations of CTAB, a cationic surfactant .....	16
<b>Figure 2.12</b> Methane hydrate formation rate at different concentrations of ENP, a nonionic surfactant.....	17
<b>Figure 2.13</b> Foam generation during hydrate dissociation with SDS as a promoter ..	17
<b>Figure 2.14</b> Methane consumption during hydrate growth: (●) Pure water, (●) Arginine, (●) Valine and (●) SDS.....	18
<b>Figure 2.15</b> Bar plots showing the effect of amino acids and reactor configurations on (a) Productivity and (b) Hydrate yield, column arranging from left to right: water (stirred), 0.3 wt% leucine (stirred), 0.3 wt% (unstirred) and 0.3 wt% leucine (hybrid) .....	19

<b>Figure 2.16</b> Morphology of methane hydrate formation using 0.3 wt% leucine with a focus on methane bubble .....	20
<b>Figure 2.17</b> Hydrate dissociation using 0.3 wt% leucine as a promoter.....	20
<b>Figure 2.18</b> Hydrate phase equilibrium curve of methane-water system and methane-water-5.56 mol% THF system .....	21
<b>Figure 2.19</b> Methane uptake at the end of hydrate formation at different pressure ....	23
<b>Figure 2.20</b> Comparison of methane uptake profiles during hydrate formation obtained in the presence and absence of L-Arginine in water-THF solution at the condition of 7.2 MPa and 293.2 K.....	24
<b>Figure 2.21</b> Comparison of methane uptake profiles for the different systems studied at 9.5 MPa and 298.2 K .....	24
<b>Figure 2.22</b> (a) $^{13}\text{C}$ NMR spectra of the methane-pyrrolidine hydrate and (b) tuning pattern at various concentrations of pyrrolidine solution .....	25
<b>Figure 3.1</b> Schematic of (a) experimental apparatus, (b) cross-section of window crystallizer, and (c) cross-section of sapphire crystallizer .....	28
<b>Figure 4.1</b> Hydrate phase equilibrium of pure methane hydrates and mixed methane-THF hydrates together with the experimental data obtained in this study for the mixed methane-pyrrolidine and methane-THF hydrate system.....	34
<b>Figure 4.2</b> Typical P-T profiles for an experiment with 5.56 mol% of (a) pyrrolidine and (b) THF at 4.5 MPa .....	36
<b>Figure 4.3</b> Average methane uptake profile of mixed methane-pyrrolidine hydrates (P1 – P3 experiments) together with the visual observations for an experimental trial P1 .....	41
<b>Figure 4.4</b> Morphological observation of methane hydrate formation using 5.56 mol% pyrrolidine as a promoter at 8 MPa and 285.2 K in the sapphire crystallizer ...	43
<b>Figure 4.5</b> Temperature and pressure driving forces of the experiments at 285.2 and 292.2 K and 8 MPa of both methane-pyrrolidine and methane-THF hydrate system.	46

<b>Figure 4.6</b> Comparison of the induction time (IT) and the normalized rate of hydrate formation ( $NR_{15}$ ) with different promoters at the same driving force ((a) and (b)) and the same experimental condition ((a) and (c)) .....	47
<b>Figure 4.7</b> Average methane uptake profiles from methane hydrate formation with different promoters at the same driving force (line (a) and (b)) and the same experimental condition (line (a) and (c)) .....	48
<b>Figure 4.8</b> Comparison of the average time to reach 90% of methane uptake ( $t_{90}$ ) and the average final methane uptake with different promoters at the same driving force ((a) and (b)) and the same experimental condition ((a) and (c)).....	49
<b>Figure 4.9</b> Morphology observations of P1, T1, and T5 trials during the methane hydrate formation in the presence of (a) pyrrolidine at 285.2 K, (b) THF at 292.2 K, and (c) THF at 285.2 K.....	50
<b>Figure 4.10</b> Average normalized methane recovery during the decomposition process in the presence of different promoters under different initial conditions .....	53
<b>Figure 4.11</b> Morphology observations of P1, T2 and T5 trials during the decomposition process in the presence different promoters .....	54

# CHAPTER 1

## INTRODUCTION

Natural gas is a promising source of energy, which mainly contains methane approximately more than 90% together with a small percentage of other hydrocarbon gases. According to its high methane composition, natural gas emits less greenhouse gases (e.g. CO<sub>2</sub>, CO, SO<sub>2</sub>) during combustion compared with other fossil sources (Demirbas, 2010). This reason brings natural gas to become one of the cleanest fossil fuels, and thus resulting in an increase in its demand. Based on the world energy outlook, natural gas was estimated to grow 1.9% per year from 2020 to 2025 (EIA, 2020). This leads to a great attention in the technology for natural gas storage and transportation in a large scale. Nowadays, several conventional approaches to store natural gas are compressed natural gas (CNG) and liquefied natural gas (LNG) (Lozano-Castelló *et al.*, 2002). Even though these approaches have been widely used, they still have some drawbacks. For CNG, natural gas is pressurized at a very high pressure resulting in the safety concern. For LNG, the gas needs to be stored at a very low temperature (its boiling point at about -161°C) resulting in the requirement of a costly cooling system (Sapag *et al.*, 2010; Wang *et al.*, 2010). Recently, a promising alternative approach, where natural gas is kept in the form of solid, was discovered. This novel approach, known as solidified natural gas (SNG), stores the gas using clathrate hydrate technology. SNG has several advantages to overcome the conventional approaches including higher volumetric energy storage, moderate temperature and pressure operation, and being extremely safe (Veluswamy *et al.*, 2018).

Hydrates or clathrate hydrates are ice-like solid crystalline and non-stoichiometric compounds that form when small guest gas molecules (methane, ethane, propane, etc.) come in contact with water molecules at certain conditions of pressure and temperature. The guest molecules get incorporated into hydrogen bonded framework cages, formed by water molecules, in which Van der Waals forces between them stabilize their structure (Englezos, 1993; Sloan, 2003; Sloan and Koh, 2008). The thermodynamic formation conditions and the size of guest gas molecules

determine the hydrate structure. There are three common structures of hydrates: structure I (sI), structure II (sII), and hexagonal structure H (sH) (Sloan and Koh, 2008). Besides, clathrate hydrates are able to store approximately 170 volumes of gas per one volume of hydrate at STP. This characteristic property is the key factor to adopt clathrate hydrates to store natural gas and also emphasizes that SNG has an ability to become one of the candidates for natural gas storage and transportation. (Hao *et al.*, 2008; Veluswamy *et al.*, 2018).

However, clathrate hydrates still have some limitations such as a slow formation rate and a requirement of low formation temperature. In order to overcome the slow formation kinetics, an increase in the dispersion of gas into liquid solution along with a decrease in the interfacial tension between gas-liquid interface have been considered. The kinetic promoters have been used to achieve those objectives resulting in the increase in mass transfer between those two phases, and thus improve their kinetics. Surfactants have been reported as an effective kinetic promoter (Ganji *et al.*, 2007; Zhang *et al.*, 2007; Zhong and Rogers, 2000). Nevertheless, foam is generated during the dissociation process, which is undesirable for large scale applications. Amino acids are alternative kinetic promoters to overcome the foam formation. Several studies show that amino acids can be used to promote hydrate formation kinetically (Bavoh *et al.*, 2019; Bavoh *et al.*, 2018; Jeenuang *et al.*, 2021; Veluswamy *et al.*, 2017).

Using kinetic promoters, methane hydrates still form sI; hence, the conditions at a low temperature together with a high pressure are required. To shift the hydrate formation to moderate conditions, thermodynamic promoters have to be applied. Tetrahydrofuran (THF) is one of the most notable thermodynamic promoters and forms sII hydrates with water molecules, where THF occupies the large cages leaving the small cages vacant for methane molecules (Prasad *et al.*, 2009). This characteristic plays an important role to change methane hydrate structure from sI to sII, resulting in the capability to operate at milder conditions. It can be confirmed by Papadimitriou *et al.* (2009) that the pressure stability at 293 K of methane hydrates was reduced from 19 MPa to only 2 MPa in the presence of THF. Moreover, Beheshtimaal and Haghtalab (2018) found that the highest methane uptake was achieved at the stoichiometric ratio (5.56 mol%) of THF. There was no significant difference of



methane uptake in the methane-THF hydrates not only at different temperatures (283.2 K, 288.2 K and 293.2 K) but at different pressures (4 MPa, 6 MPa and 8 MPa), as reported by Veluswamy *et al.* (2016b) and Inkong *et al.* (2019), respectively. Bhattacharjee *et al.* (2020) also found that methane-THF hydrates could occur at the condition of 298.2 K. These results ensure that THF is an effective sII thermodynamic promoter.

Many researchers have attempted to improve the methane hydrate formation. Pyrrolidine is another chemical having an analogous structure with THF. The structure of pyrrolidine and THF is presented in Figure B1 in the Supporting Information. In comparison, the heteroatom of pyrrolidine is nitrogen, while the one of THF is oxygen. Not only does pyrrolidine have very similar structure to THF, but its amine group is also identical with amino acid. According to this reason, this promoter might have both functions of thermodynamic and kinetic improvement at the same time. However, there are only few studies related to using pyrrolidine as a promoter (Shin *et al.*, 2012). Therefore, the objectives of this work are to investigate the roles of pyrrolidine on methane hydrate formation in terms of thermodynamics, kinetics, and morphology and to compare with those of THF.

## CHAPTER 2

### LITERATURE REVIEW

#### 2.1 Natural Gas

Natural gas is a naturally occurring hydrocarbon gas, usually formed deep underground in areas around oil and coal. It primarily composes of methane ( $\text{CH}_4$ ) over 90% but also has some other hydrocarbon gases such as ethane, propane, etc. It may contain nitrogen, carbon dioxide, and trace amounts of water. Nowadays, natural gas is one of the most widely used forms of energy in almost all sectors including heating, electricity generation, and vehicle fuels. That is because combustion of natural gas is clean and emits less greenhouse gases (e.g.,  $\text{SO}_2$ ,  $\text{CO}$ ,  $\text{CO}_2$ ) than all other fossil fuels.

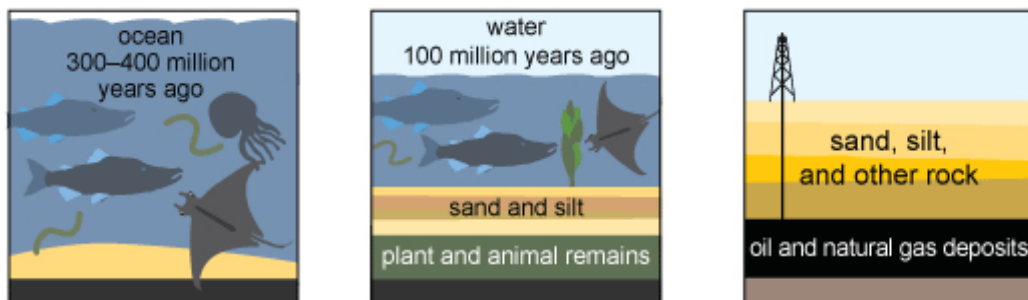


**Figure 2.1** Natural gas formation (U.S. Energy Information Administration).

Natural gas is considered as a non-renewable fossil fuel. It comes from the decomposition of organic matter such as the dead remains of tiny sea animals and plants that died million years ago. These remains sank to the bottom of the oceans and were buried under the sedimentary rocks. With the long periods of time, these rocks became more thicker resulting in the subject of those remains to massive pressure. Combination of pressure and heat from the earth makes them turn to petroleum (oil) and gas. Finally, natural gas is trapped in the layers of rock (Demirbas, 2010).

## 2.2 Natural Gas Storage and Transportation

Natural gas is the fastest-growing primary energy source in the forecast (EIA, 2020) since it is a cleaner fuel than oil and coal. On average, the combustion of natural gas releases up to 50% and 33% less greenhouse gas in comparison with coal and oil, respectively. Moreover, the combustion of other fossil fuels emits other hazardous air pollutants such as particulate matter, whereas natural gas hardly does. This brings natural gas to become one of the most effective fossil fuels. Therefore, the efficient technology for natural gas storage and transportation is very important (C2ES, 2013). The most common way for natural gas storage and transportation is transporting through pipeline, but it is not practical for a long distance.

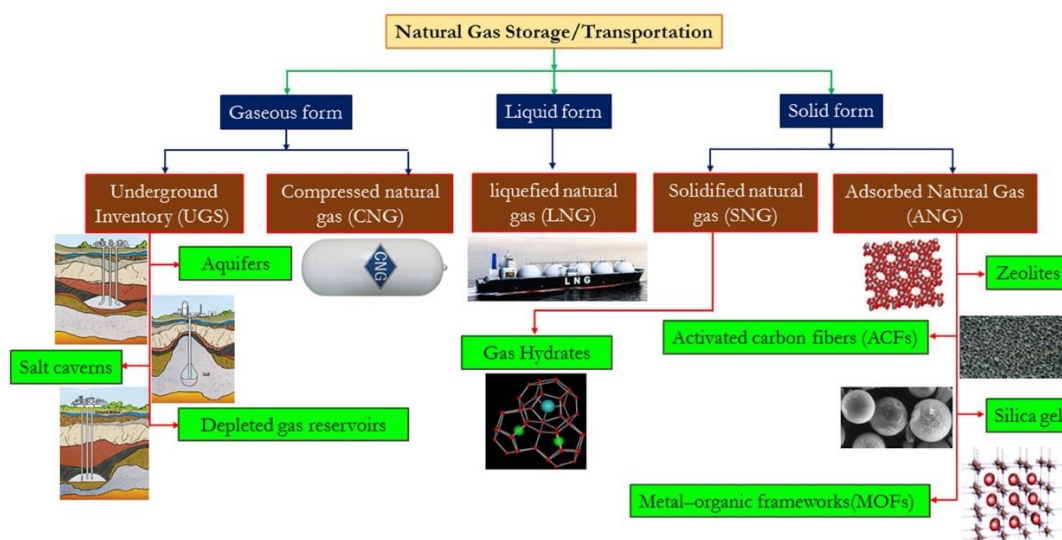


**Figure 2.2** Natural gas storage and transportation (Veluswamy *et al.*, 2018).

### 2.2.1 Compressed Natural Gas (CNG)

With the use of CNG, natural gas must be stored as a compressed supercritical fluid at ambient temperature at maximum pressure about 20 – 25 MPa (3,000 – 3,600 psi) reaching a density 230 times higher than the one obtained at STP conditions. However, a major disadvantage is the safety concern. Modifications of thick-walled tanks and complex safety valves would be required due to the massive pressure.

### 2.2.2 Liquefied Natural Gas (LNG)

Natural gas is stored as a liquid at the boiling point (-161°C) in a cryogenic tank under a pressure of 0.1 MPa. LNG has the volume about 600 times smaller than natural gas at STP. Thus, this makes it easier to store and transport due to the smaller volume. Although this method has widely used, its disadvantages are about boil-off gas along with a costly pressurization and cooling system (Sapag *et al.*, 2010; Wang *et al.*, 2010).

### 2.2.3 Adsorbed Natural Gas (ANG)

ANG is another possible approach by adsorbing natural gas to porous materials such as graphene, activated carbon, metal organic frameworks (MOFs), etc. This approach requires relatively low pressure (3.5 – 4 MPa, much lower than in CNG) at room temperature. However, it is also noted that this technology is not well-developed and is still at scientific level since the price of some porous materials is expensive (Lozano-Castelló *et al.*, 2002; Sapag *et al.*, 2010).

Recently, a promising alternative approach, where natural gas is kept in the form of solid was discovered. This novel approach, known as solidified natural gas (SNG), stores the gas using clathrate hydrate technology. SNG has several advantages that are able to overcome the conventional methods including:

- (i) Hydrate formation is environmentally friendly as only water and a very low concentration of promoter (if any) are needed.
- (ii) Almost complete recovery is achieved by simple thermal stimulation.
- (iii) Moderate temperature and pressure conditions are required.
- (iv) It is very safe due to the fact that its nature and structure are non-explosive (Veluswamy *et al.*, 2018).



3243175980

CU IThesis 6271006063 thesis / rev: 19072564 14:31:51 / seq: 40

## 2.3 Gas Hydrates

### 2.3.1 Early History

In 1778, study of gas hydrates was started by Priestly, whereas the chemistry of them was discovered in 1810 by Sir Humphrey Davy who found that an aqueous solution could form ice-like crystals (Davy, 1811). After that, gas hydrates had been an academic curiosity for almost five decades.

Table 2.1 shows the history timeline of methane gas hydrates. By the end of 19th century, Villard was the first scientist who discovered methane gas hydrates that often formed well above the freezing point of water (Arora *et al.*, 2015). Gas hydrates then have become more interesting for further study.

**Table 2.1** History timeline of methane gas hydrates (Modified from Demirbas (2010))

Year	Progress
1888	Villard was the first scientist who discovered methane gas hydrates.
1934	Hydrates found to clog gas pipelines
1964	Scientists found methane hydrates existed in Siberian permafrost.
1970	Methane hydrates were found in ocean sediments.
1992	Beginning of intentionally looking for methane gas hydrates deposits

In 1930s, natural gas miners began to complain of an ice-like material plugging pipelines. This material was determined that it was not pure ice, but ice wrapped around methane. That makes methane hydrates receive a great attention to solve plugging problem. In 1960s, it was the first time that scientists found naturally occurring gas hydrates, as they had never been found before (Harris, 2009). In 1970s, methane hydrates were found in ocean sediments based on seismic observations. Then, in 1992, the Ocean Drilling Program began intentionally identifying for hydrate deposits and sample were brought for study.

### 2.3.2 Definition

Hydrates or clathrate hydrates are ice-like solid crystalline and non-stoichiometric compounds that form when small guest gas molecules meet water molecules at a certain condition of pressure and temperature. Hydrates are crystals where water molecules form the cage framework through hydrogen bond and the guest molecules (methane, ethane, propane, etc.) are trapped inside. The structure of these molecules is stabilized by Van der Waals forces (Englezos, 1993; Sloan, 2003; Sloan and Koh, 2008). In the past, studies of gas hydrate originally focused on ensuring the flow in pipelines, which often plugged with the hydrates. After the deep-sea exploration, scientists found the massive amount of natural gas hydrates in the ocean sediments. Per unit volume, hydrates contain tremendous amount of gas. That is, for example, they can store about 170 volumes of gas per volume of hydrate. As can be seen in Figure 2.3, methane hydrates easily burn under atmospheric pressure and then convert back to methane and water.



**Figure 2.3** Methane hydrate pellet samples (Pictures taken in The Petroleum and Petrochemical College, Chulalongkorn University, Bangkok, Thailand).

### 2.3.3 Structure and Characteristics of Hydrates

The hydrogen bonds of water molecules form framework of cages that are filled by small guest gas molecules. Water molecules itself cannot be in those cages (McCarthy and Jordan, 2006). Depending on the size of guest molecules along with thermodynamic formation conditions, hydrates occur different structures. There are three common structures of hydrates including structure I (sI), structure II (sII) and hexagonal structure H (sH) (Sloan and Koh, 2008). The summaries are shown in Figure 2.4 and Table 2.2.

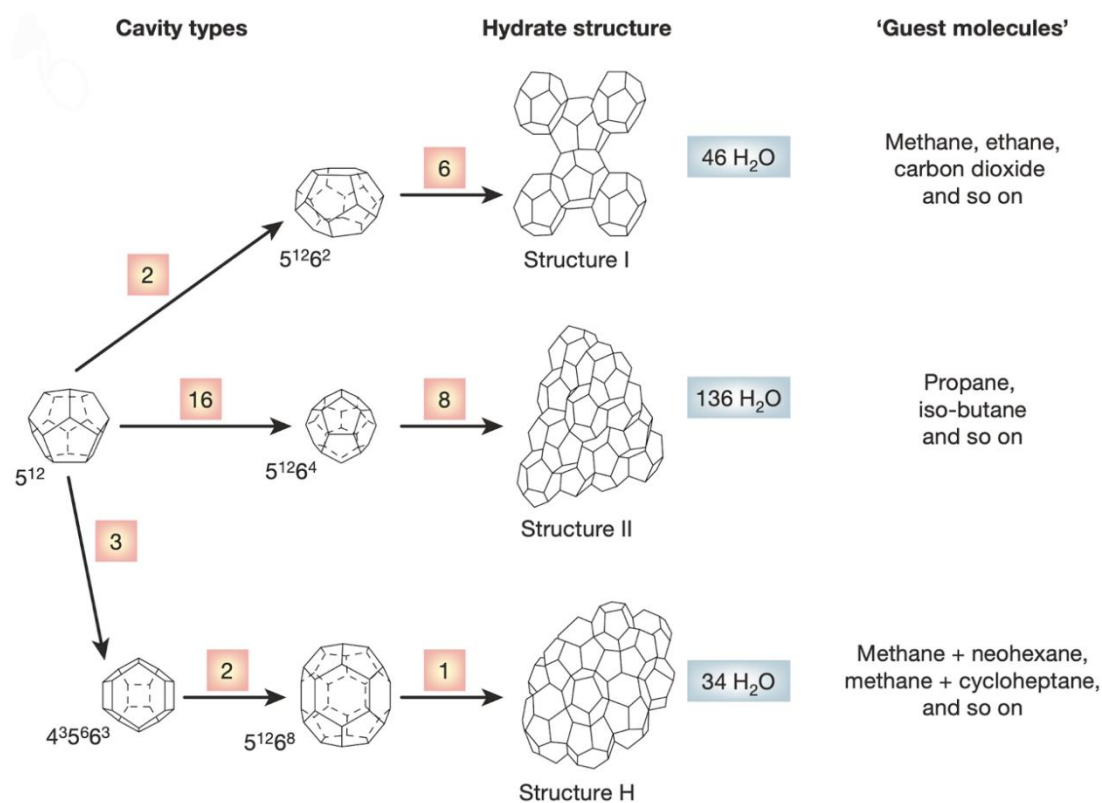


**Figure 2.4** Three common structure of hydrates: sI, sII and sH (Sloan, 2003).

**Table 2.2** Characteristics of three hydrate structures (Data modified from Sloan and Koh (2008))

Crystal structure	sI		sII		sH		
	Small	Large	Small	Large	Small	Medium	Large
<b>Description</b>	$5^{12}$	$5^{12}6^2$	$5^{12}$	$5^{12}6^4$	$5^{12}$	$4^35^66^3$	$5^{12}6^8$
<b>Numbers of cavities</b>	2	6	16	8	3	2	1
<b>Number of water molecules</b>	46		136		34		
<b>Crystal system</b>	Cubic		Cubic		Hexagonal		

### 2.3.3.1 Structure I (sI)

In structure I, one unit cell contains 46 water molecules by forming 8 total cages including 2 small pentagonal dodecahedrons ( $5^{12}$ ) combining with 6 tetrakaidecahedrons ( $5^{12}6^2$ ). Therefore, the radius of these cavities increases to 0.433 nm (Schicks, 2018). The sI hydrates can accommodate up to 8 guest molecules and are usually formed by smaller molecules including methane, ethane, and carbon dioxide.

### 2.3.3.2 Structure II (sII)

The unit cell of sII is composed by 136 water molecules by forming 24 cages including 16 small pentagonal dodecahedrons ( $5^{12}$ ) and 8 large hexakaidecahedrons ( $5^{12}6^4$ ). This makes the radius of these cavities increases to 0.473 nm. Due to the 24 void cages, the sII hydrates can contain 24 guest gas molecules. They are usually formed by larger molecules such as propane and i-butane (Harrison, 2010).

Therefore, a unit cell of an sI hydrates consists of 46 water molecules creating 2 small cages and 6 large cages. A unit cell of sII hydrates consists of 136 water molecules creating 16 small cages and 8 large cages. Filling guest molecules at least 70% can stabilize both structure and are known as simple hydrates.



### 2.3.3.3 Structure H (sH)

A unit cell of sH hydrates consists of 34 water molecules by forming 6 cages including 3 pentagonal dodecahedrons ( $5^{12}$ ), 2 irregular dodecahedrons ( $4^35^66^3$ ) and 1 icosahedron ( $5^{12}6^8$ ). sH is the only structure, which contains three-type cavities as mentioned above. With this reason, sH hydrates can contain large guest gas molecules (e.g. cycloheptane) in large cages and the smaller ones (e.g. methane) in the small cages (Demirbas, 2010; Schicks, 2018).

### 2.3.4 Clathrate Hydrates

When clathrate hydrates form, water molecules form the network cages creating two types (or three types in sH) of cages being together. The sI hydrates and sII hydrates consist of a cubic lattice whereas the sH hydrates consist of a hexagonal lattice. After the clathrate hydrates are formed, the guest molecules are going to be trapped inside those cages, formed by water. There is no relationship between guest molecules and water molecules except only the Van der Waals forces that stabilize their structure (Luzi *et al.*, 2008; Marboeuf *et al.*, 2011).

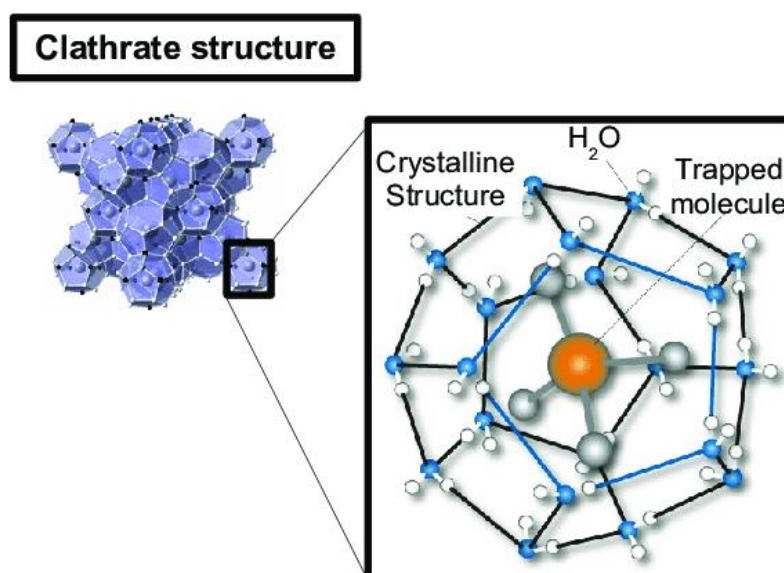


**Figure 2.5** Schematic view of clathrate hydrate structure (Marboeuf *et al.*, 2011).

## 2.4 Hydrate Formation

Hydrate formation is considered as a crystallization process. It can be divided into two steps. The first step is hydrate nucleation, where small clusters take place and then further develop into hydrate nuclei. After the nuclei reach their stable structure, a hydrate growth process starts continuously (Khurana *et al.*, 2017).

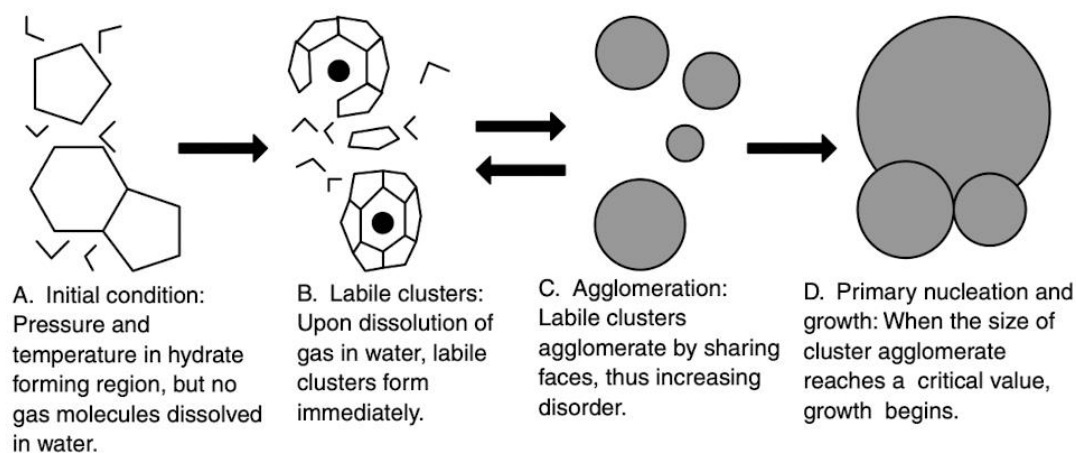


**Figure 2.6** Conceptual of hydrate nucleation (Aman and Koh, 2016).

### 2.4.1 Hydrate Nucleation

Hydrate nucleation is a phenomenon that small clusters of guest molecules and water occur and then expand to be stable hydrate nuclei. The formation of hydrate nuclei usually takes place at the interface due to higher concentration of both water and guest molecules and higher surface contact between two phases (Khurana *et al.*, 2017). Since the nucleation step requires a specific condition, the major factor of the nucleation is the magnitude of driving force which is dependent on pressure and temperature (Skovborg and Rasmussen, 1994).

Several hypotheses have been performed to understand this mechanism including labile cluster hypothesis, nucleation at interface hypothesis and local structuring nucleation hypothesis (Sloan and Koh, 2008), as shown in Figure 2.6.

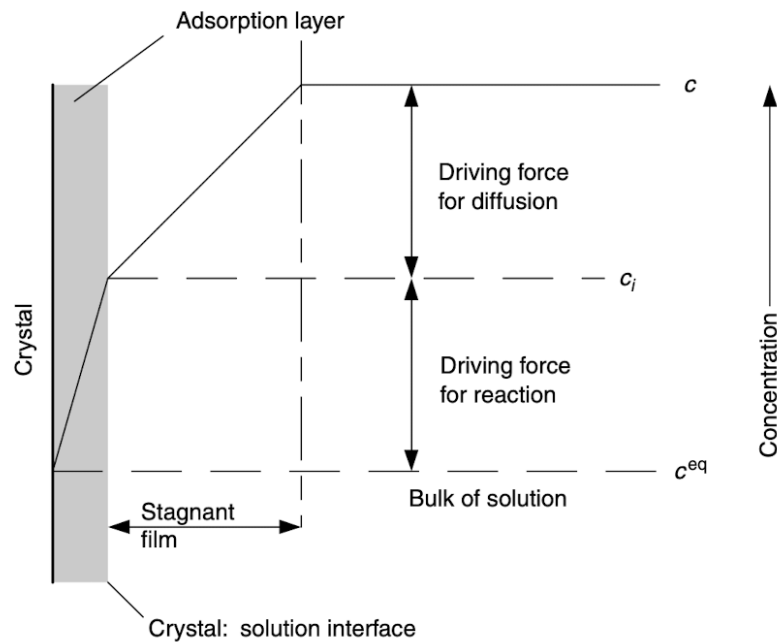


**Figure 2.7** Conceptual model of hydrate growth process: mass transfer, diffusion of gas into stagnant layer and the incorporation into hydrate (Sloan and Koh, 2008).

#### 2.4.2 Hydrate Growth

A continuous growth process starts after the hydrate nuclei obtain the critical size reaching their stable structure. During this process, a significant amount of gas gets incorporated in hydrate phase. According to Englezos *et al.* (1987) model, hydrate growth process is a three-step process. All steps are shown in Figure 2.7. The first one is the transport of the gas molecule to liquid phase (mass transfer). The second step is the diffusion of gas molecule through a stagnant liquid followed by the last step which is the incorporation of gas molecule into water framework. Due to the strong exothermic reaction of hydrate growth, heat and mass transfer also plays an important role in this step.

## 2.5 Hydrate Dissociation

Hydrate dissociation is an endothermic process, in which external energy is required for breaking down Van der Waals forces and hydrogen bonds between guest and water molecules. After the completion of dissociation, the hydrate lattices revert to water and guest molecules. Figure 2.8 shows three common methods that can be applied to dissociate the hydrates including depressurization, thermal stimulation and chemical injection.

Depressurization can be done by reducing the pressure to be outside the stability region. This makes hydrates not be able to endure such environment, and thus hydrates are completely dissociated. In contrast with the first method, thermal stimulation can be done by increasing temperature to above the phase equilibrium temperature. For chemical injection, some chemicals must be injected to inhibit the formation of hydrates. This is achieved by shifting the phase equilibrium curve to higher pressure and lower temperature.

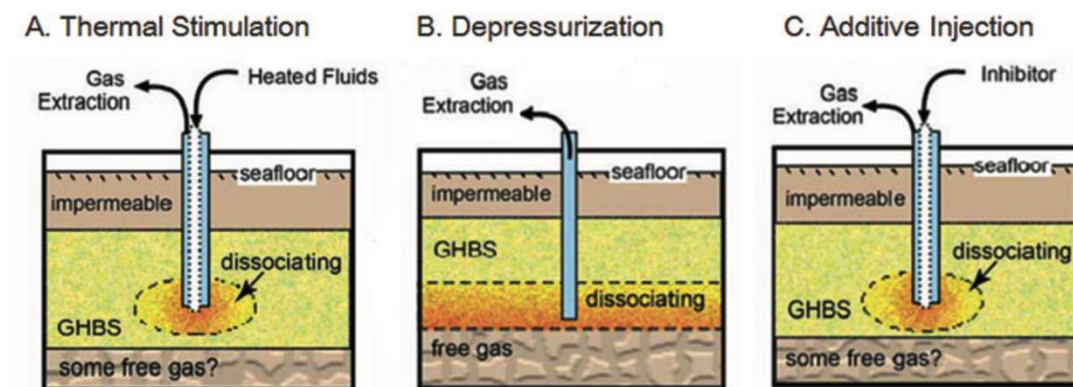


**Figure 2.8** Three common methods for the hydrate dissociation (Kumar and Linga, 2017).

## 2.6 Hydrate Promoter

### 2.6.1 Kinetic Promoter

The kinetic promoters are used to increase in the dispersion of gas into liquid solution along with decrease in interfacial tension between gas-liquid interface during hydrate formation. According to their functions, mass transfer between two phases is increased resulting in the kinetic improvement.

#### 2.6.1.1 Surfactants

Ganji *et al.* (2007) studied the effect of different types of surfactants including anionic surfactant, cationic surfactant, and non-ionic surfactant. In comparison with other surfactants, sodium dodecyl sulfate (SDS), which is an anionic surfactant, was proposed to be the best surfactant-based kinetic promoter. SDS even at a low concentration had the highest performance to accelerate the hydrate formation rate, as shown in Figure 2.9 to Figure 2.12. However, Figure 2.13 shows that surfactants can generate foam during hydrate dissociation, which is not preferable.

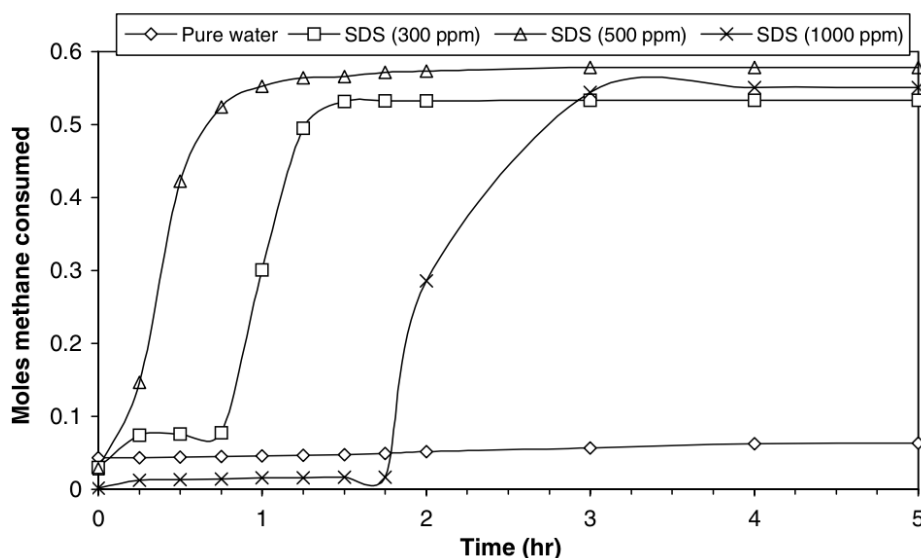


**Figure 2.9** Methane hydrate formation rate at different concentrations of SDS, an anionic surfactant (Ganji *et al.*, 2007).

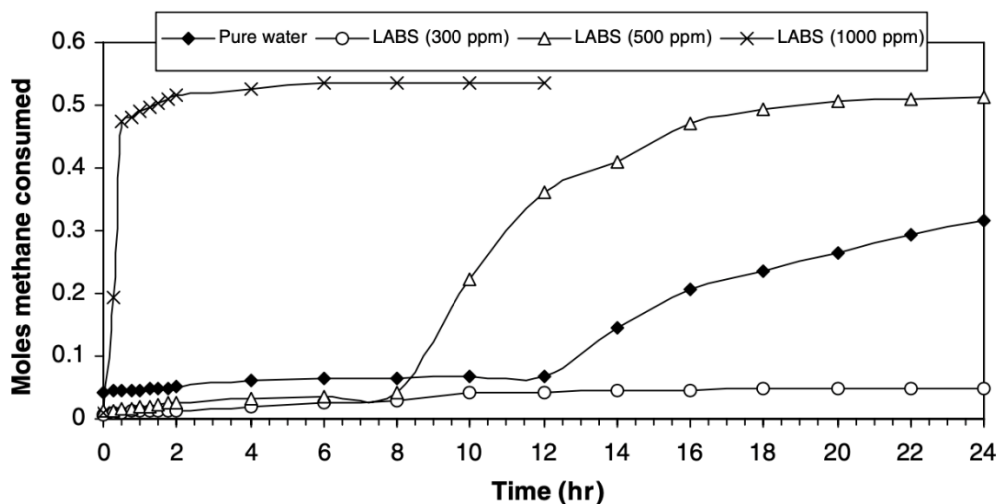


**Figure 2.10** Methane hydrate formation rate at different concentrations of LABS, an anionic surfactant (Ganji *et al.*, 2007).

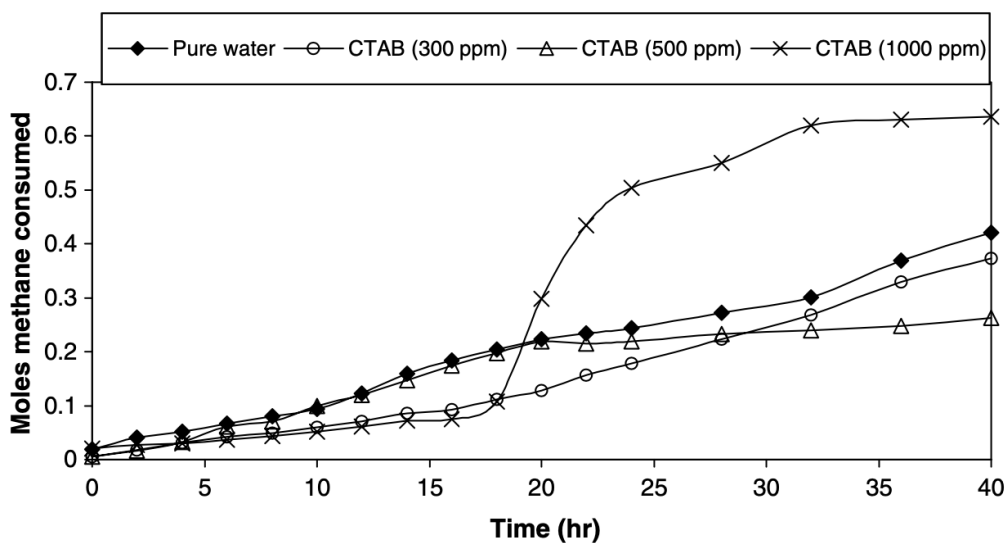


**Figure 2.11** Methane hydrate formation rate at different concentrations of CTAB, a cationic surfactant (Ganji *et al.*, 2007).



3243175980

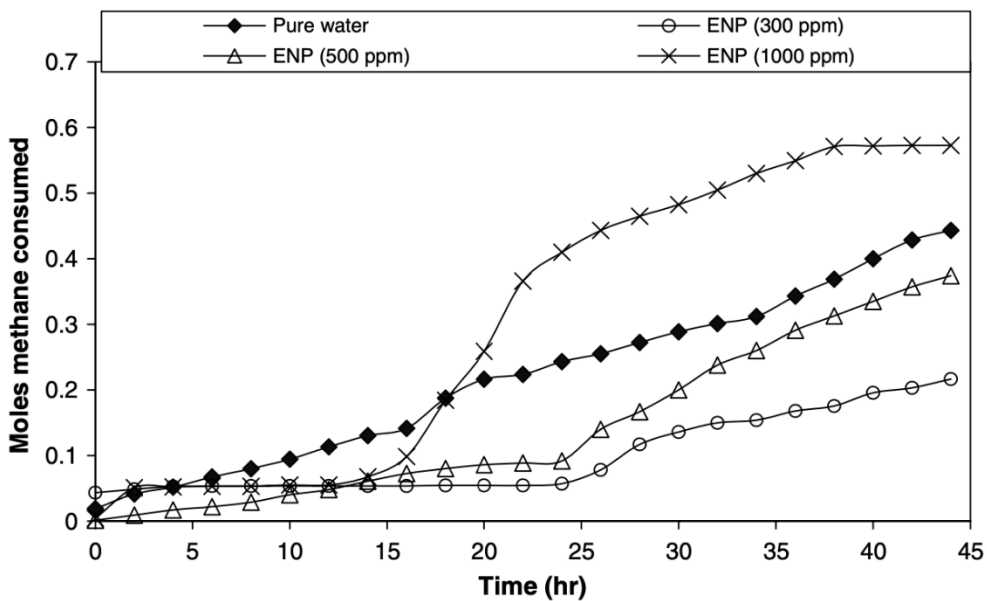


**Figure 2.12** Methane hydrate formation rate at different concentrations of ENP, a nonionic surfactant (Ganji *et al.*, 2007).

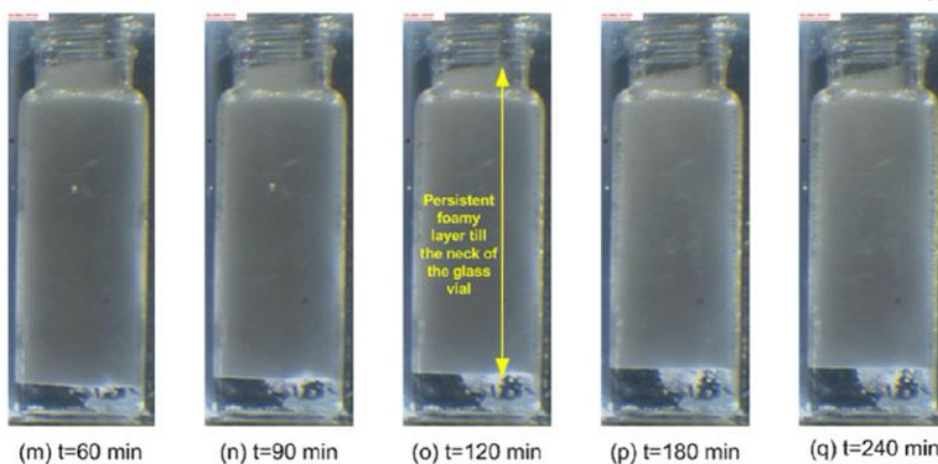


**Figure 2.13** Foam generation during hydrate dissociation with SDS as a promoter (Modified from Veluswamy *et al.* (2016a)).

### 2.6.1.2 Amino Acids

In order to overcome the drawbacks of surfactants, amino acids are promising kinetic options, as they are eco-friendly and easy to biodegrade. Especially, amino acids do not generate foam during gas recovery.

It was mentioned in many studies that amino acids have the potential to accelerate the hydrate formation kinetics. Bavoh *et al.* (2018) reported the effect of two amino acids (valine and arginine) on the kinetics of methane hydrate formation. As shown in Figure 2.14, it was found that the presence of both amino acids gave higher rate of hydrate formation compared to the system with only pure water. Interestingly, methane consumption of the system with amino acids was higher than the system with SDS.

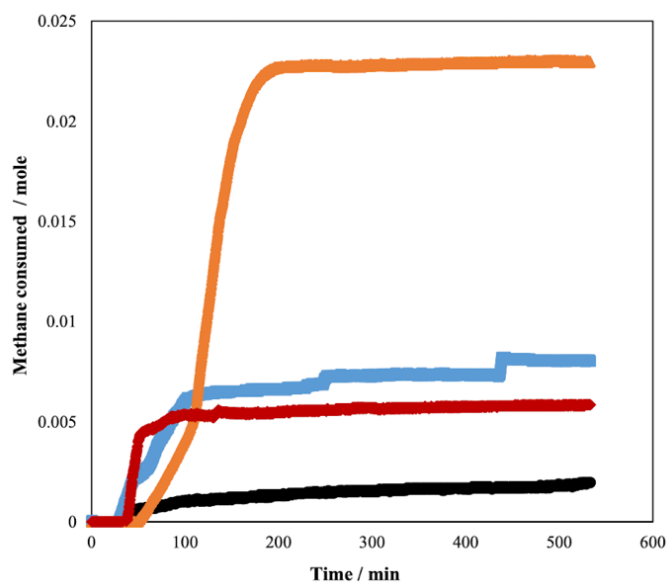


**Figure 2.14** Methane consumption during hydrate growth: (●) Pure water, (●) Arginine, (●) Valine and (●) SDS (Bavoh *et al.*, 2018).

The study by Veluswamy *et al.* (2017) also showed the promotion of selected amino acid (leucine) on the methane hydrate formation kinetics. Figure 2.15 shows that approximately five times higher productivity and the highest hydrate yield of 80% was achieved by using 0.3 wt% leucine solution, while the yield of pure water system was only 13%. It was further observed that there was no significant difference on the productivity and hydrate yield between stirred and



unstirred systems. It could be confirmed that amino acids can be applied as kinetic promoters without any reactor configuration.

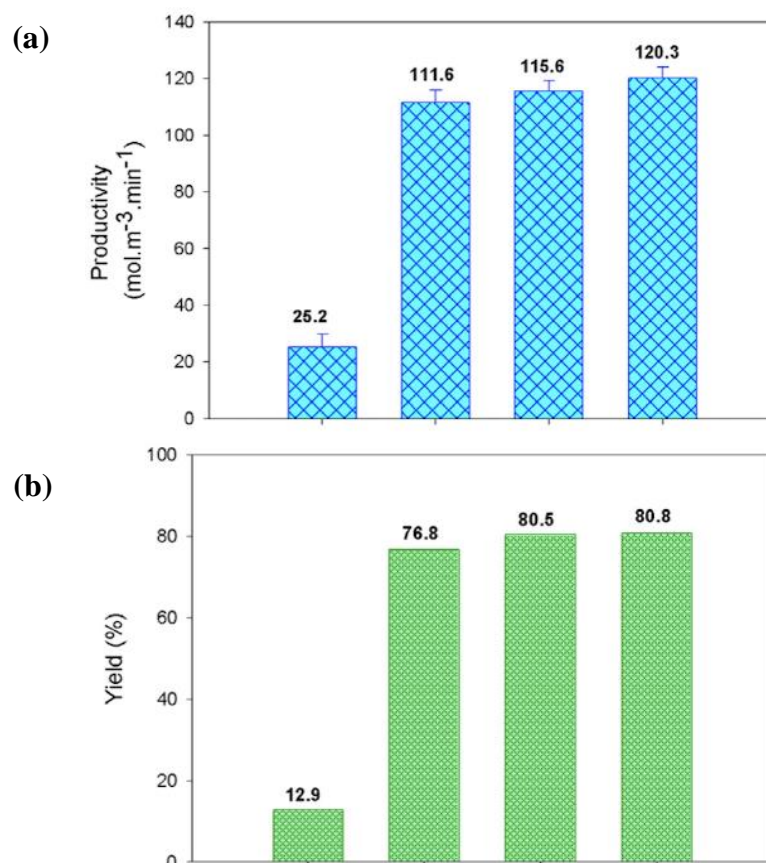


**Figure 2.15** Bar plots showing the effect of amino acids and reactor configurations on (a) Productivity and (b) Hydrate yield, column arranging from left to right: water (stirred), 0.3 wt% leucine (stirred), 0.3 wt% (unstirred) and 0.3 wt% leucine (hybrid) (Veluswamy *et al.*, 2017).

Moreover, the morphology of methane hydrate formation in the presence of leucine was investigated by Veluswamy *et al.* (2016a). They found an interesting characteristic called ‘methane bubble’ in the bulk solution with the assistance of ‘breathing effect’, as shown in Figure 2.16. These phenomena attributed to enhance methane hydrate formation kinetics. As mentioned earlier, unlike surfactants, amino acids do not generate foam formation. This can be confirmed by Figure 2.17.

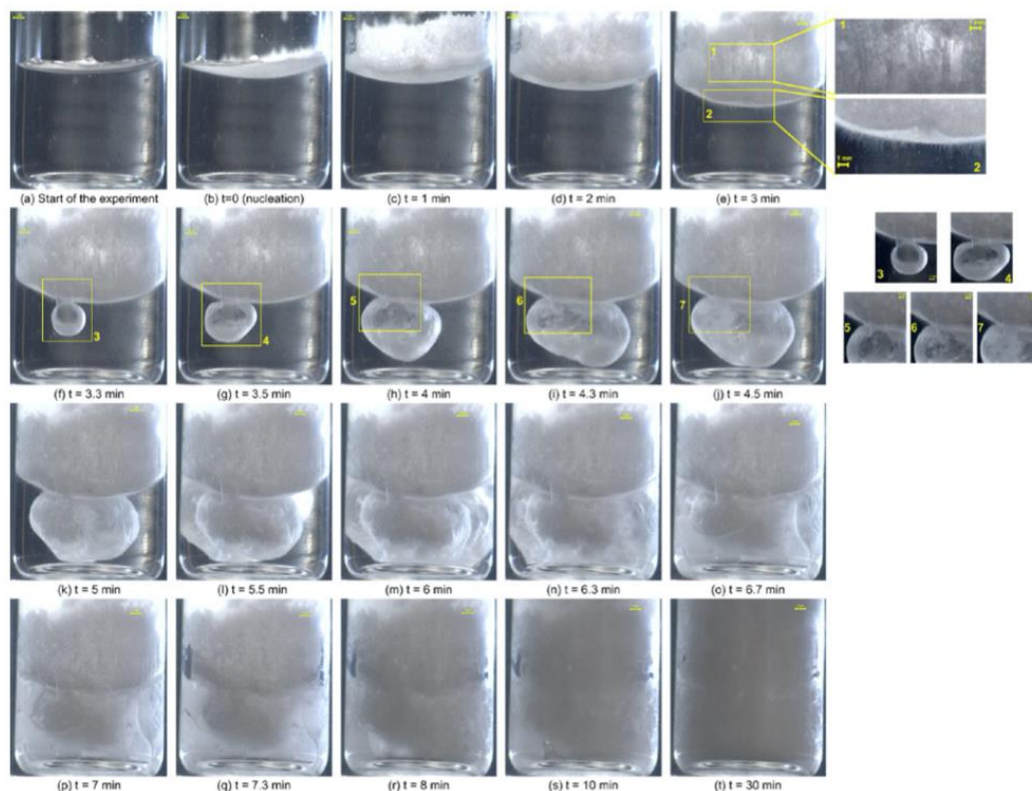


**Figure 2.16** Morphology of methane hydrate formation using 0.3 wt% leucine with a focus on methane bubble (Veluswamy *et al.*, 2016a).

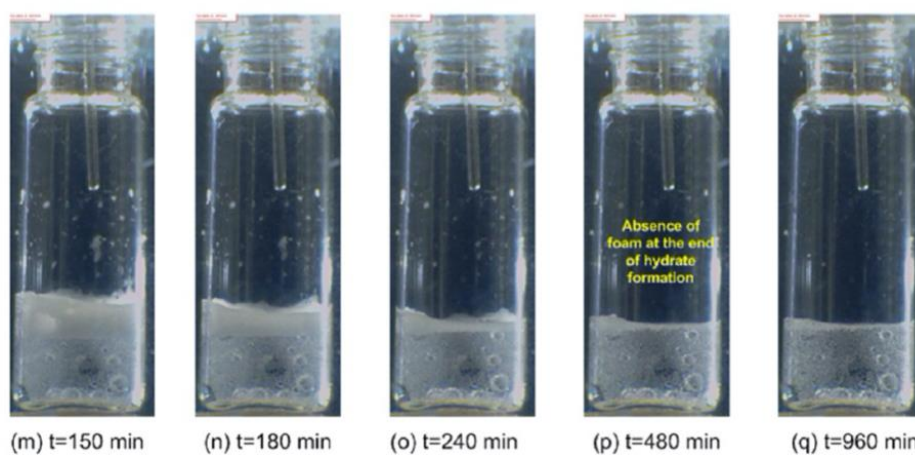


**Figure 2.17** Hydrate dissociation using 0.3 wt% leucine as a promoter (Modified from Veluswamy *et al.* (2016a)).

## 2.6.2 Thermodynamic Promoter

The hydrates form structure I when kinetic promoters are applied. These promoters do not change equilibrium curve; consequently, the condition of low temperature and high pressure is still necessary. To shift the hydrate formation condition to moderate condition, thermodynamic promoters are required.

### 2.6.2.1 Tetrahydrofuran (THF)

THF has been reported as one of the most well-known thermodynamic promoters. Lee *et al.* (2012) investigated the effect of THF on the mixed methane-THF hydrate equilibrium curve. The results are shown in Figure 2.18. The presence of THF shifts phase equilibrium curve on methane-THF-water system to far lower pressure and higher temperature compared to only methane-water system. This can be explained by Prasad *et al.* (2009) study that THF occupies in the large cages ( $5^{12}6^4$ ) leaving the small cages ( $5^{12}$ ) available for methane molecules. This characteristic plays an important role to change hydrate structure from sI to sII, resulting in the capability to operate at milder condition.

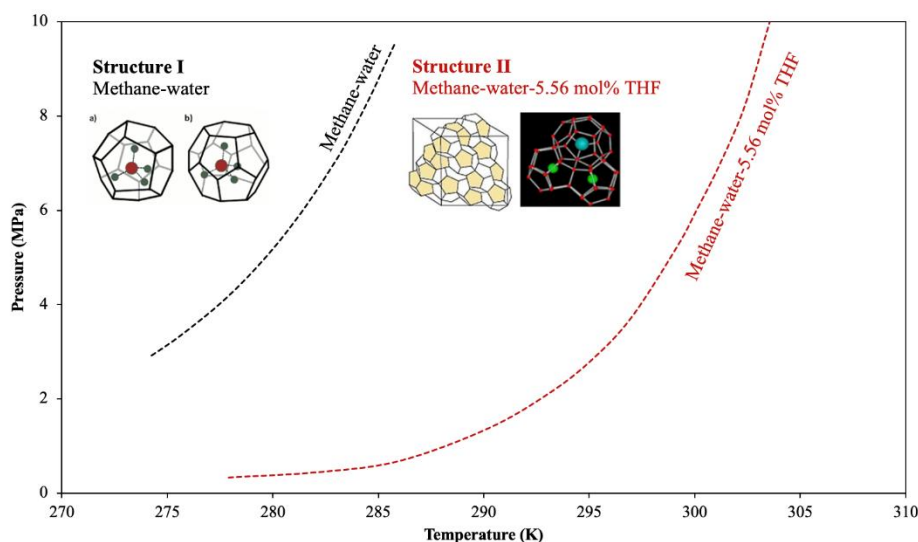


**Figure 2.18** Hydrate phase equilibrium curve of methane-water system and methane-water-5.56 mol% THF system (both equilibrium data were from Nakamura *et al.* (2003) and Lee *et al.* (2012), respectively).

To investigate the roles of THF on methane uptake at different temperature and pressure, Veluswamy *et al.* (2016b) studied the effect of temperature on methane hydrate formation. They reported that there was no significant difference of methane gas uptake under different temperatures (283.2 K, 288.2 K and 293.2 K). However, as shown in Table 2.3, the rate of formation decreased with the increased temperature due to lower driving force of temperature.

**Table 2.3** Average data for results of hydrate formation for experiments conducted at 7.2 MPa and different temperatures (Veluswamy *et al.*, 2016b)

Exp.N	Temp. (K)	Induction time (min)	Time for 90%completion (min)	Methane uptake (kmol/mol)	Rate of methane uptake (kmol m <sup>-3</sup> h <sup>-1</sup> )		
					Stage 1	Stage 2	Stage 3
<b>A1</b>	283.2	5.55	46.22	3.82	5.500		
<b>A2</b>		(±9.05)	(±1.39)	(±0.166)	(±0.208)		
<b>A3</b>							
<b>B1</b>	288.2	1.11	112.44	3.68	1.840	2.098	
<b>B2</b>		(±0.70)	(±3.15)	(±0.166)	(±0.276)	(±0.144)	
<b>B3</b>							
<b>C1</b>	293.2						
<b>C2</b>							
<b>C3</b>		25.80	402.05	3.81	0.204	0.530	1.005
<b>C4</b>		(±17.72)	(±96.25)	(±0.082)	(±0.077)	(±0.093)	(±0.155)
<b>C5</b>							

Inkong *et al.* (2019) also found the similar tendency that gas uptake is about the same despite different pressures (4 MPa, 6 MPa and 8 MPa), as shown in Figure 2.19. This could be attributed to effective heat distribution to the surrounding. Similarly, lower driving force of pressure resulted in lower rate of formation.

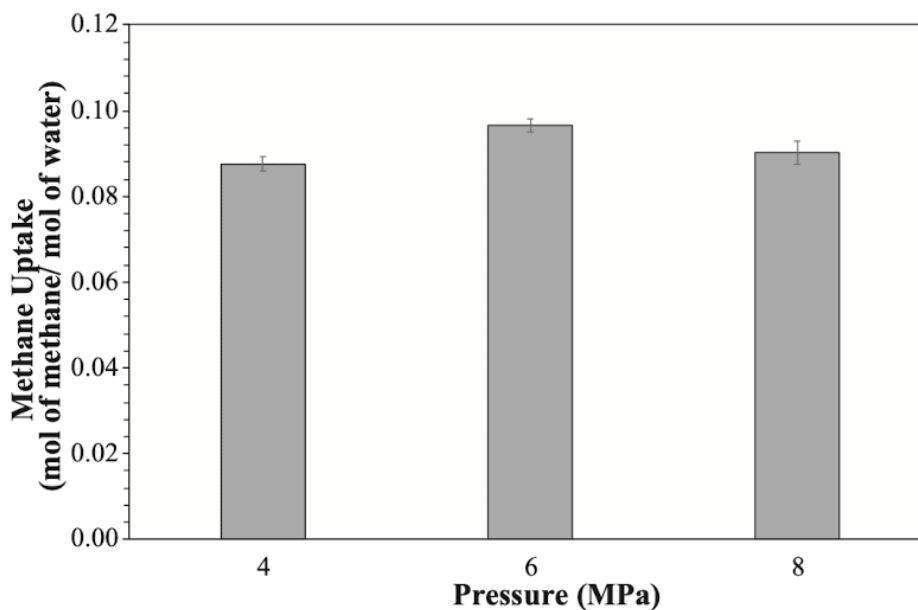


**Figure 2.19** Methane uptake at the end of hydrate formation at different pressure (Inkong *et al.*, 2019).

Moreover, Kumar *et al.* (2019a) found out that the addition of amino acids, which are the kinetic promoters, into the system with THF, which is the thermodynamic promoters, can improve the rate of hydrate formation. The results were satisfied since the rate was much higher than the system with only THF, as shown in Figure 2.20. This is due to the synergism effect between them.

Besides higher rate of hydrate formation, Bhattacharjee *et al.* (2020) reported that adding some amino acids into methane-THF hydrate system could improve methane uptake, as shown in Figure 2.21. In addition, methane-THF hydrates could occur at the ambient condition of 298.2 K. These results ensure that THF is an effective sII thermodynamic promoter.

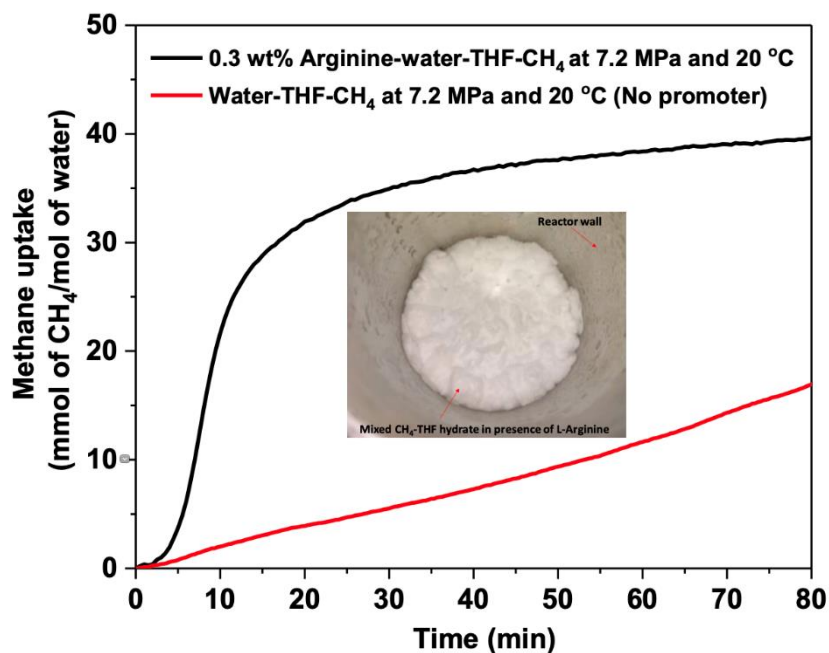


**Figure 2.20** Comparison of methane uptake profiles during hydrate formation obtained in the presence and absence of L-Arginine in water-THF solution at the condition of 7.2 MPa and 293.2 K (Kumar *et al.*, 2019a).

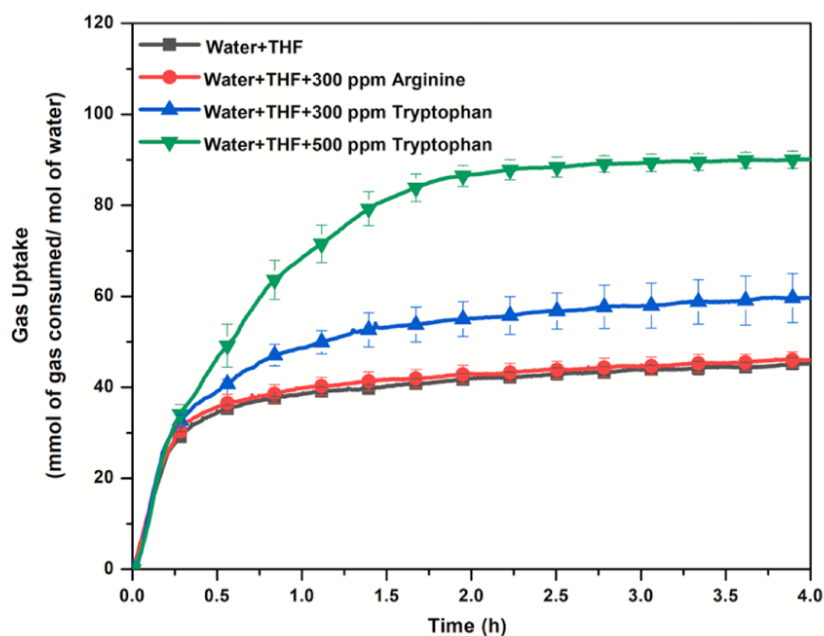


**Figure 2.21** Comparison of methane uptake profiles for the different systems studied at 9.5 MPa and 298.2 K (Bhattacharjee *et al.*, 2020).



3243175980

CD IThesis 6271006063 thesis / revv: 19072564 14:31:51 / seq: 40

### 2.6.2.2 Pyrrolidine

Pyrrolidine has an analogous structure with THF. The only difference is its heteroatom, where nitrogen atom belongs to pyrrolidine and oxygen atom belongs to THF. The study of using pyrrolidine as a methane hydrate promoter was done by Shin *et al.* (2012). They reported that, at stoichiometric ratio (5.56 mol%), all pyrrolidine molecules were trapped in large cages and only methane molecules were inside the small cages owing to their molecular size. About 13 methane molecules could be stored per unit cell. This number is greater than that of sI hydrates.

Moreover, at a low concentration of pyrrolidine, they also found ‘the inclusion phenomena’, of which the methane molecules could be inside large cages together with pyrrolidine molecules. This phenomenon slightly disappeared at higher concentration, as shown in Figure 2.22.

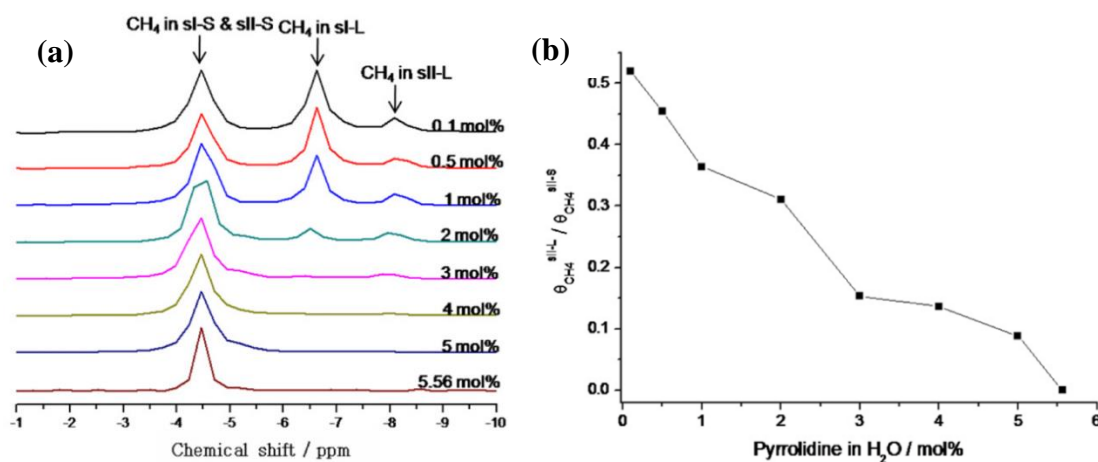


**Figure 2.22** (a)  $^{13}\text{C}$  NMR spectra of the methane-pyrrolidine hydrate and (b) tuning pattern at various concentrations of pyrrolidine solution (Shin *et al.*, 2012).

# CHAPTER 3

## EXPERIMENTAL

### 3.1 Materials and Equipment

#### 3.1.1 Chemicals

1. Ultra-high purity methane gas (99.99% purity from Linde Public Company, Thailand)
2. Pyrrolidine (99% purity from Sigma-Aldrich, Singapore)
3. Tetrahydrofuran (AR grade from RCL Labscan, Thailand)
4. Deionized water

#### 3.1.2 Hydrate Formation / Dissociation Apparatus

1. Crystallizer (CR)
2. Reservoir (R)
3. Personal computer (PC)
4. Pressure transmitter (PT) (Model 68073 from Cole Parmer, Singapore)
5. K-type thermocouple (SL heater, Thailand)
6. Controllable water bath (Model RC-20 from Daeyang, Korea)
7. Magnetic stirrer



## 3.2 Experiment Procedures

### 3.2.1 Experiment Apparatus

The schematic of gas hydrate experimental setup is shown in Figure 3.1a. All kinetic experiments were batch type and were operated in a window crystallizer (CR), Figure 3.1b, made from 316 stainless steel, which had a maximum working pressure of 20 MPa. The crystallizer had an internal volume of approximately 80 cm<sup>3</sup> and was fitted with two sapphire windows in order to allow visual observation inside. Moreover, in order to clearly observe the morphology, a 50 cm<sup>3</sup> high-pressure sapphire crystallizer (CR), Figure 3.1c, was also applied in this work. The 50 cm<sup>3</sup> reservoir (R) was also connected to both systems. Both CR and R were submerged in a temperature-controlled bath. An external refrigerator (ER) (Model RC-20, Labtech, India) was employed to maintain the experimental temperature by circulating the mixture of ethylene glycol and water in the ratio of 1:4. The system pressure was measured by pressure transmitter (PT) (Cole Parmer, Model 68073, Singapore) with the range of 0–3,000 psig and 0.13 % global error. An analog pressure gauge (Swagelok, USA) was also used along with pressure transmitter to monitor pressure in the system. The reactor temperature was measured by K-type thermocouple (SL heater, Thailand). Both pressure transmitter and thermocouple were connected to a Data logger (DL) (AI210, Wisco Industrial Instruments, Thailand), which was connected to a personal computer (PC). The temperature and pressure data were recorded every 10 seconds using the software provided by Wisco Industrial Instruments, Thailand. For morphological observation, the images and video during hydrate formation and dissociation were captured by a camera (VC) (Optika, Model C-HP, Italy) with the macro camera lens (VS Technology Corporation, Japan).



3243175980

CU Theses 6271006063 thesis / rev: 19072564 14:31:51 / seq: 40

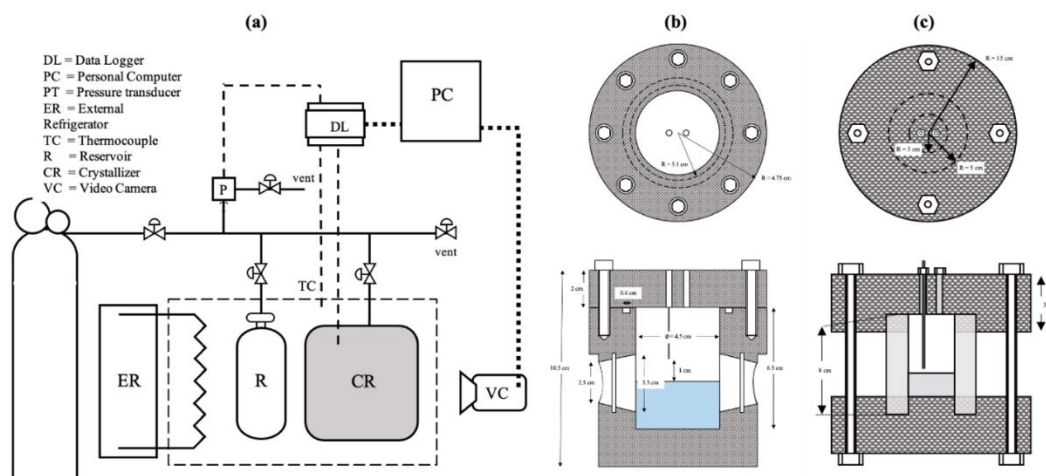


**Figure 3.1** Schematic of (a) experimental apparatus, (b) cross-section of window crystallizer, and (c) cross-section of sapphire crystallizer (modified from (Siangsai *et al.*, 2015)).

### 3.2.2 Experiment Procedure for Thermodynamic Studies

In this work, the procedure for determining the hydrate phase equilibrium followed from Zheng *et al.* (2018) study by using the isochoric pressure search method. After 35 cm<sup>3</sup> of the 5.56 mol% solution was added into the window crystallizer, it was flushed with methane gas three times to ensure that there was no air in the system and then methane gas was pressurized to a desired pressure. At this time, the crystallizer was also maintained at 308.2 K by an external refrigerator. After pressurization, a 300 rpm stirring rate was started using a magnetic stirrer. Once the pressure was stabilized, the crystallizer was cooled to a low temperature (277.2 K) to form hydrates. The stabilization of pressure for at least 1 hour indicated that the hydrate formation was completed. The hydrates could also be observed through the sapphire windows. Stirring was stopped at this point. The crystallizer then was heated in a step of 0.5 K/h, and the system was allowed to stabilize before next step heating. This procedure was done repeatedly until the completion of last hydrate crystal decomposition. The temperature at this last crystal decomposition was recorded as the first estimate of the equilibrium temperature ( $T_{e1}$ ).

Afterwards, the second cycle was conducted following the similar procedure. The difference is that the crystallizer was heated in a step of 0.1 K/h when

the temperature got close to  $T_{e1}$ . During the procedures mentioned above, the pressure and temperature profiles were tracked. The equilibrium temperature was specified by the intersection point of cooling and heating curves, obtained from the second cycle. This ensures that the error of the equilibrium temperature is within 0.1 K.

### 3.2.3 Experiment Procedure for Kinetic and Morphology Studies

The effects of using pyrrolidine and THF as a promoter on kinetics and morphology for methane hydrate formation were investigated. The procedure was similar for both studies. 35 cm<sup>3</sup> or 7 cm<sup>3</sup> of 5.56 mol% solution was added into the window crystallizer or the sapphire crystallizer, respectively. After that, the crystallizer was flushed with methane gas three times in order to remove the air. The system was also set at a desired temperature by using an external refrigerator. Methane gas was then introduced to the system at 8 MPa. During hydrate formation process, pressure and temperature were recorded every 10 seconds until there was no further pressure drop for at least 1 hour. For morphology study, the images and videos were also recorded. The calculation procedure was the same as (Siangsai *et al.*, 2015) and Inkong *et al.* (2019) studies. For further details, the gas uptake was achieved by Equation 3.1.

$$\Delta n_{H,\downarrow} = n_{H,0} - n_{H,t} = \left( \frac{PV}{ZRT} \right)_{G,0} - \left( \frac{PV}{ZRT} \right)_{G,t} \quad (3.1)$$

where  $\Delta n_{H,\downarrow}$  = moles of gas consumed during the hydrate formation, (mole)

$n_{H,t}$  = moles of methane gas at time  $t$ , (mole)

$n_{H,0}$  = moles of methane gas at the beginning, (mole)

$P$  = pressure inside the crystallizer, (atm)

$T$  = temperature inside the crystallizer, (K)

$V$  = the volume of gas phase in the system, (cm<sup>3</sup>)

$Z$  = compressibility factor Pitzer's correlation (Smith *et al.*, 2005)

$R$  = the universal gas constant of 82.06 cm<sup>3</sup>•atm/mol•K

Subscript of  $G,0$  and  $G,t$  represents the gas phase at time zero and time  $t$ , respectively.

The normalized initial rate of hydrate formation ( $NR_t$ ) for the first  $t$  minutes from the beginning of hydrate growth can be achieved by the Equation 3.2.

$$NR_t = \frac{R_t}{V_{\text{water}}} \quad (3.2)$$

where  $V_{\text{water}}$  = volume of water added in the crystallizer, ( $\text{m}^3$ )  
 $R_t$  = the rate of hydrate growth, ( $\text{kmol/hr}$ ), which was calculated by fitting the average gas uptake during the hydrate growth at each experimental condition versus time for the first  $t$  minutes after the induction time, using the least-squares method.

After the completion of hydrate formation, hydrates were dissociated through the thermal stimulation by increasing the temperature to 308.2 K, which is out from the hydrate stable region. The beginning of the dissociation process was marked as time zero. During this process, the pressure in the system was rising owing to the melting of hydrates. After hydrates completely dissociated, the temperature was steady at 308.2 K, and the pressure was constant. The system was allowed to maintain at that constant pressure for at least 1 hour before the end of overall process. The total moles of methane gas released during the dissociation process was calculated by Equation 3.3. Moreover, the methane recovery was calculated by Equation 3.4.

$$\Delta n_{H,\uparrow} = n_{H,t} - n_{H,0} = \left( \frac{PV}{zRT} \right)_{G,t} - \left( \frac{PV}{zRT} \right)_{G,0} \quad (3.3)$$

where  $\Delta n_{H,\uparrow}$  = moles of gas released during the hydrate dissociation, (mole)  
 $n_{H,t}$  = moles of methane gas at time  $t$ , (mole)  
 $n_{H,0}$  = moles of methane gas at the beginning, (mole)  
 $P$  = pressure inside the crystallizer, (atm)  
 $T$  = temperature inside the crystallizer, (K)  
 $V$  = the volume of gas phase in the system, ( $\text{cm}^3$ )  
 $Z$  = compressibility factor  
 $R$  = the universal gas constant of  $82.06 \text{ cm}^3 \cdot \text{atm/mol} \cdot \text{K}$

Subscripts of  $G,0$  and  $G,t$  represent the gas phase at time zero and time  $t$ , respectively.

$$\% \text{methane recovery} = \frac{(\Delta n_{H,\uparrow})}{(\Delta n_{H,\downarrow})_{\text{End}}} \times 100 \quad (3.4)$$

where  $\Delta n_{H,\uparrow}$  = moles of gas released from the hydrate dissociation, (mole)  
 $\Delta n_{H,\downarrow}$  = moles of gas consumed from the hydrate formation, (mole)



3243175980

CU Theses 6271006063 thesis / rcv: 19072564 14:31:51 / seq: 40

## CHAPTER 4

### RESULTS AND DISCUSSION

This work investigated the roles of pyrrolidine on the methane hydrate formation via the detailed thermodynamic and kinetic studies and also elucidated the formation mechanism through a visual observation by morphology study. All experiments were done using both THF and pyrrolidine in order to compare and discuss their roles in the hydrate formation. The concentration of both promoters used in all experiments was 5.56 mol%. This concentration was reported as a stoichiometric ratio corresponding to the full occupancy of promoter in the large cages of sII hydrates with the molar ratio of water to promoter = 1:17 (Chang *et al.*, 2020). This number comes from the fact that one unit cell of sII hydrates composes of 136 water molecules forming 8 large cages (Sloan, 2003; Sloan and Koh, 2008). The formation conditions for kinetic and morphology study were all chosen in the sII hydrate region only so that there is no possibility for methane to form sI hydrates.

#### 4.1 Thermodynamic Study: Phase Equilibrium Measurement for Methane-pyrrolidine and Methane-THF Hydrate System

Due to the lack of the equilibrium data of mixed methane-pyrrolidine hydrates, the equilibrium conditions were first determined before conducting the kinetic and morphology studies. The equilibrium data of mixed methane-THF hydrates were also obtained in this work although these data are readily available in many studies. This was done to confirm the reliability of the experimental apparatus and method. The results show that the equilibrium data are in good agreement with those from Lee *et al.* (2012). The summary of the thermodynamic phase equilibrium conditions for mixed methane-pyrrolidine and mixed methane-THF hydrates at 5.56 mol% concentration is presented in Table 4.1. Together with the table, the plot of the equilibrium data is also shown in Figure 4.1. The data indicate that pyrrolidine has the potential to be a thermodynamic promoter for the methane hydrate formation. The pure methane hydrates require more severe conditions for the formation than those of

mixed methane-pyrrolidine hydrates. Specifically, the equilibrium pressure for the formation of pure methane hydrates at 285.2 K MPa is 8.8 MPa, while that for mixed methane-pyrrolidine hydrates is only 2.4 MPa. Thus, this can confirm that the addition of pyrrolidine can significantly lower the hydrate formation pressure at a given temperature.

**Table 4.1** Equilibrium data obtained in this study for the mixed methane-pyrrolidine hydrate and methane-THF hydrate systems

System	Equilibrium conditions	
	Pressure (MPa)	Temperature (K)
Mixed methane- pyrrolidine	8.48	295.2
	7.09	293.8
	5.90	292.6
	4.35	289.9
	3.17	287.3
	1.86	282.8
Mixed methane-THF	8.80	303.2
	7.34	301.6
	5.96	300.3
	4.45	298.3
	2.89	295.2
	1.96	292.8

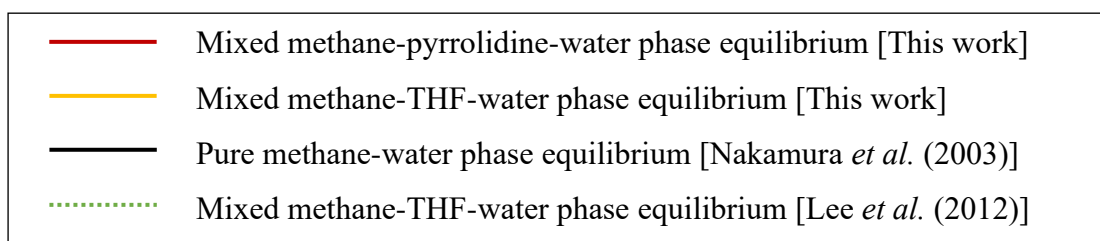
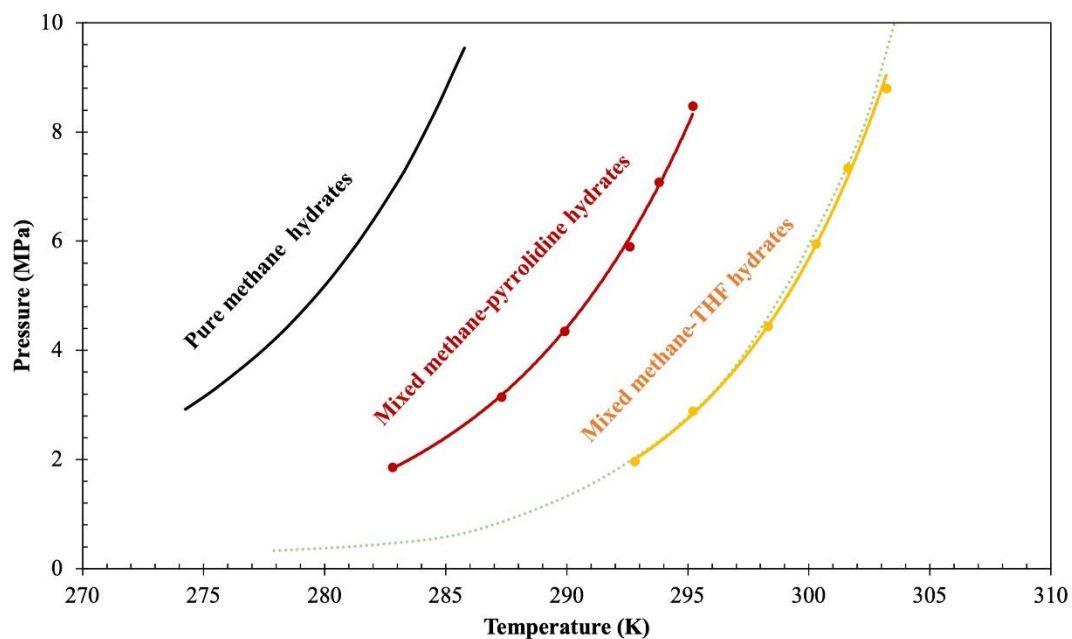


**Figure 4.1** Hydrate phase equilibrium of pure methane hydrates (Nakamura *et al.*, 2003) and mixed methane-THF hydrates (Lee *et al.*, 2012) together with the experimental data obtained in this study for the mixed methane-pyrrolidine and methane-THF hydrate system.

It has been reported in many literatures that THF aids to alleviate the clathrate hydrates to form at milder conditions. With the molecular level study by in situ Raman characterization, Kumar *et al.* (2019b) reported the cage occupancy wherein large cages were dominated by THF and small cages by methane. Similarly, Shin *et al.* (2012) analyzed the structure of mixed methane-pyrrolidine hydrates using both Raman spectroscopy and powder x-ray diffraction (p-XRD). They confirmed that pyrrolidine also gave the similar structure to THF, and pyrrolidine occupied the large cages leaving the small ones for methane molecules. It should be noted that this is the major reason for this promotion effect that the phase equilibrium is shifted to a lower



pressure and higher temperature (Mech and Sangwai, 2016; Sum *et al.*, 1997). However, in comparison with THF, pyrrolidine does not shift the equilibrium curve as much as THF. The difference in the equilibrium temperature is approximately 8 K. This is due to the fact that thermodynamic promoters perform better if they can form hydrates themselves without any help from the guest gas molecules (Tohidi *et al.*, 1997). THF has been proven that it can form hydrates by itself (Gough and Davidson, 1971), whereas pyrrolidine needs the help from methane molecules for the enclathration (Shin *et al.*, 2012). That makes methane molecules less independent and more difficult to be trapped inside the small cages of hydrate structure for mixed methane-pyrrolidine system.

The typical P-T profiles for an experiment with 5.56 mol% of pyrrolidine and THF at the pressure of 4.5 MPa are shown in Figure 4.2. An isochoric pressure search method was employed at six fixed pressures of 2 MPa, 3 MPa, 4.5 MPa, 6 MPa, 7.5 MPa, and 9 MPa to create a continuous phase equilibrium curve. First, the crystallizer is maintained at a desired pressure and 308.2 K. The cooling process starts at point A, and then the pressure and temperature drop down until the hydrates form. The hydrate formation can be observed by the temperature spike, which is at point B, as the hydrate formation is an exothermic process. While the hydrates are forming, the pressure drops further to point C. At this point, no more pressure drop can be observed implying that the hydrate formation is completed. Afterwards, the crystallizer is heated to dissociate the hydrates, until point D, which is the last point of pressure and temperature that the hydrates can stand. The pressure in the system increases rapidly indicating that the hydrates start to melt. The thermodynamic equilibrium point is typically the pressure and temperature conditions, where the cooling and heating curves intersect each other, which is at point E. Finally, the temperature is increased to 308.2 K, where it is the beginning of the process.

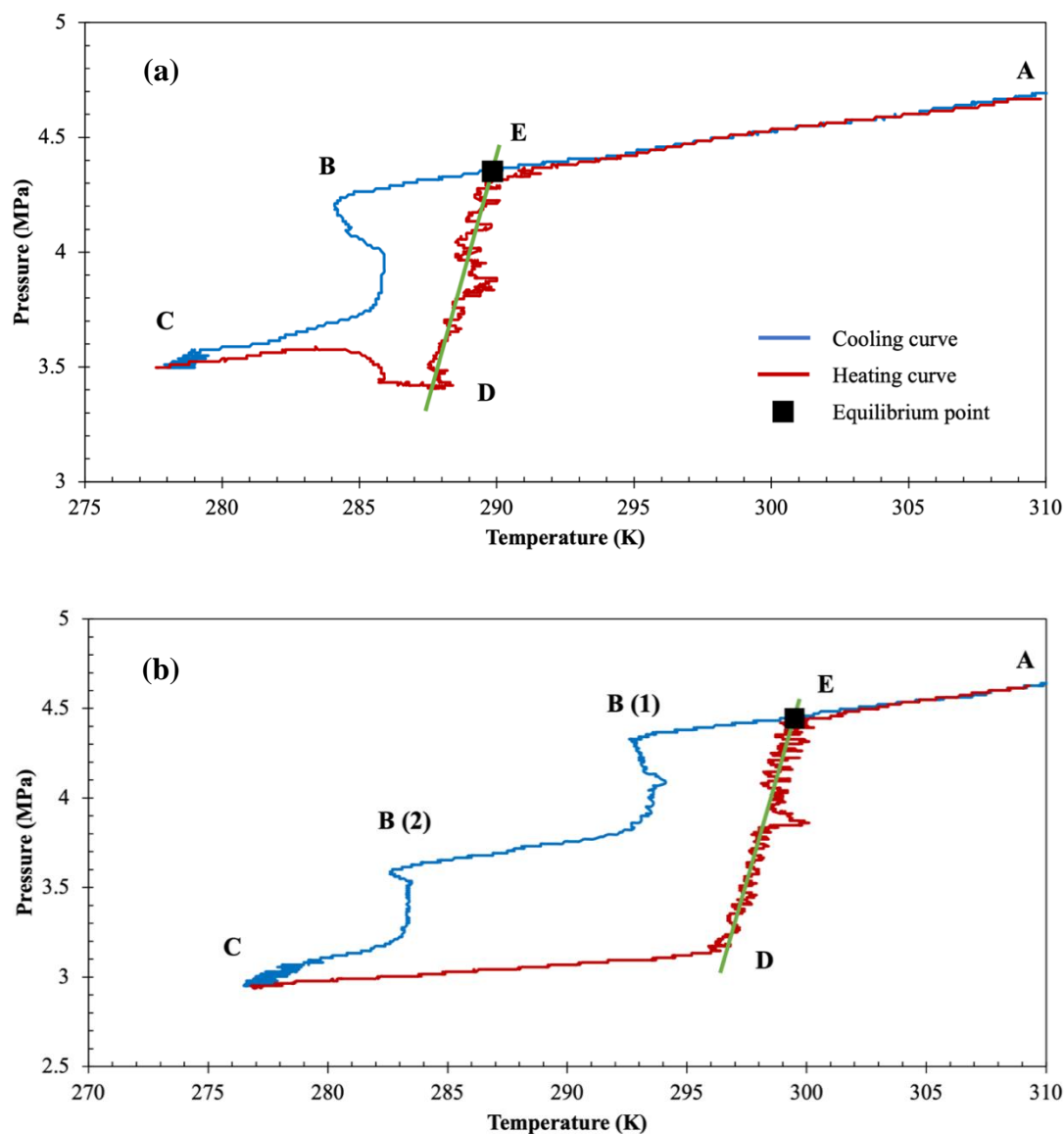


**Figure 4.2** Typical P-T profiles for an experiment with 5.56 mol% of (a) pyrrolidine and (b) THF at 4.5 MPa.

Moreover, as can be seen in the comparison between Figures 4.2a and 4.2b, the final pressures of methane-pyrrolidine and methane-THF systems are approximately 3.5 MPa and 2.9 MPa (or the methane uptake of 2.7232 and 3.7607 kmol of methane/m<sup>3</sup> of water, as shown in Figure B2 in the Supporting Information), respectively. This indicates that using THF as a promoter gives higher gas uptake than pyrrolidine. Noticeably, a multiple nucleation takes place only in the mixed methane-THF system (as illustrated at point B (1) and B (2) in Figure 4.2b), while there is only



single nucleation for the mixed methane-pyrrolidine system. The nucleation stage for both systems can be confirmed by the sharp increase in the gas uptake, shown in Figure B2 in the Supporting Information. This multiple nucleation of mixed methane-THF hydrates was also reported by Inkong *et al.* (2019) and Veluswamy *et al.* (2016b). Kadam *et al.* (2012) postulated the Single Nucleus Mechanism, which might be the reason for multiple nucleation of mixed methane-THF hydrates. They suggested that a single nucleus is formed at the induction time in a supersaturated solution, i.e., the solution is saturated with methane gas, and then undergoes secondary nucleation after reaching to a certain size. Therefore, this might also be the reason why methane gas consumption is higher in the mixed methane-THF system.

The other interesting point is that the pressure further drops during the dissociation process of the mixed methane-pyrrolidine system, indicating the secondary hydrate formation, as can be seen from Figure 4.2a between point C and D. This might be because the hydrates inside the reactor stay at an overheating state with a complex state between reversible formation and dissociation, resulting in a slow hydration as the pressure decreases along with the increase in the temperature. This is not the first time for this exclusive phenomenon to appear. Similar phenomenon was also found in other published articles (Nakane *et al.*, 2021; Shi *et al.*, 2014; Song *et al.*, 2020; Xu *et al.*, 2020). Nonetheless, the exact reasons to explain this situation are still unclear and more experiments are required for clarification. This phenomenon, however, can be observed for all experiments of the mixed methane-pyrrolidine systems but none for the other. After that, while the temperature is still increasing, the equilibrium of the system at point D is broken, so the hydrates cannot tolerate in such the environment and finally dissociate, as can be seen from the rapid increase in the pressure.



## 4.2 Kinetic and Morphology Studies

### 4.2.1 Mixed Methane-pyrrolidine Hydrate Formation under Moderate Condition

The experimental condition for mixed methane-pyrrolidine hydrates was at 285.2 K and 8 MPa. In a thermodynamic point of view, at this experimental condition, it is impossible for methane to form pure sI hydrates. Only mixed methane-pyrrolidine hydrates occur, and the structure is sII hydrates, as already proven by Raman spectroscopy and powder x-ray diffraction (p-XRD) techniques, reported by Shin *et al.* (2012). At least three cycles of hydrate formation were performed at each experiment in the kinetic and morphology studies in order to ensure the reliability. Table 4.2 provides a summary of the kinetic data of methane hydrate formation for all experiments in this study. Relevant information including the induction time (IT – the time that the hydrates first occur defining by the temperature spike during the hydrate formation), the normalized rate of methane hydrate formation in 15 minutes from the induction time ( $NR_{15}$ ), the time required to reach 90% of the final methane uptake calculated from the nucleation ( $t_{90}$ ), the methane uptake after the completion of hydrate formation (300 minutes from the nucleation), and the methane recovery percentage is reported. It should be noted that due to the batch mode operation of all experiments, the pressure of the system together with the driving force decreases as methane is trapped in the hydrate structure. Therefore, the hydrate formation ceases when the system does not have sufficient driving force to continue for the hydrate growth.



**Table 4.2** Summary of the experimental results for the methane hydrate formation of 5.56 mol% promoters at both same driving force and same experimental condition

Exp. No.	Induction Time* (min)	NR <sub>15</sub> ** (kmol/hr/m <sup>3</sup> )	t <sub>90</sub> *** (min)	Methane Uptake (kmol gas / m <sup>3</sup> of water)	% Methane Recovery
Methane + 5.56 mol% Pyrrolidine performed at 8 MPa and 285.2 K					
P1	1.00	8.5103	79.50	2.4033	96.39
P2	1.50	8.5103	76.33	2.4939	96.70
P3	0.50	8.2921	78.00	2.5381	95.17
Methane + 5.56 mol% THF performed at 8 MPa and 292.2 K					
T1	63.50	0.6505	126.83	4.6380	97.47
T2	61.67	0.6505	140.33	4.5103	98.10
T3	59.50	0.8673	145.50	4.4510	96.50
Methane + 5.56 mol% THF performed at 8 MPa and 285.2 K					
T4	9.33	11.0585	55.33	4.7343	96.21
T5	9.50	12.3595	57.00	4.5390	94.80
T6	5.33	11.9258	64.00	4.7164	96.22

\*IT (Induction Time) is the time that hydrate first occurred defining by the temperature spike during hydrate formation.

\*\*NR<sub>15</sub> is the normalized rate of hydrate formation 15 minutes from the induction time.

\*\*\*t<sub>90</sub> is the time required to reach 90% of the final methane uptake calculated from the start of experiment.

As seen from Table 4.2, it is surprising that even though the system is quiescent (unstirred configuration), pyrrolidine still gives a very short induction time of only  $1.00 \pm 0.50$  minutes implying very rapid nucleation of mixed methane-pyrrolidine hydrates. As reported by Ren *et al.* (2020), the hydrogen bond is one of the key factors and plays an important role for hydrate nucleation. It is believed that pyrrolidine has an ability to induce nearby water molecules to form the hydrate structure due to the hydrogen bond. Pyrrolidine is a secondary amine having N-H functional group; therefore, pyrrolidine itself can act as both hydrogen bond donor and acceptor at a same time (Dobrzycki *et al.*, 2015). Nitrogen atom of pyrrolidine can induce hydrogen atom of water, and its hydrogen atom can be induced by oxygen atom of water as well. Thus, it can be said that both molecules attract each other. Once pyrrolidine molecule attracts nearby water molecules, the water molecule itself is still able to pull other water molecules to create a hydrate structure framework. In addition, this pyrrolidine-induced characteristic might debilitate the hydrogen bond of water at the gas-liquid interface, resulting in a decreased interfacial free energy of the growing hydrate cluster (Asadi *et al.*, 2020). This remarkably increases the possibility of water molecules being merged into the labile clusters. Pyrrolidine here functions like a binding agent for water molecules to easily form cage hydrates. However, it should be noted that these hydrates are sII implying that pyrrolidine only helps hydrate cages to form easily at the beginning of nucleation; therefore, it does not incorporate in the water framework. In order to further understand the ability of both molecules, the simulated hydrogen bond of pyrrolidine and water is shown in Figure B3. This figure was modified from Marczak *et al.* (2017), based on the hydrogen bond donor and acceptor theory, reported by Romero Nieto *et al.* (2017). Furthermore, the addition of pyrrolidine can significantly reduce the interfacial tension of aqueous solution (Gómez-Díaz and Navaza, 2004). This increases the solubility of gas molecules contributing for methane gas to dissolve into the solution (Aman and Koh, 2016; Ganji *et al.*, 2007).

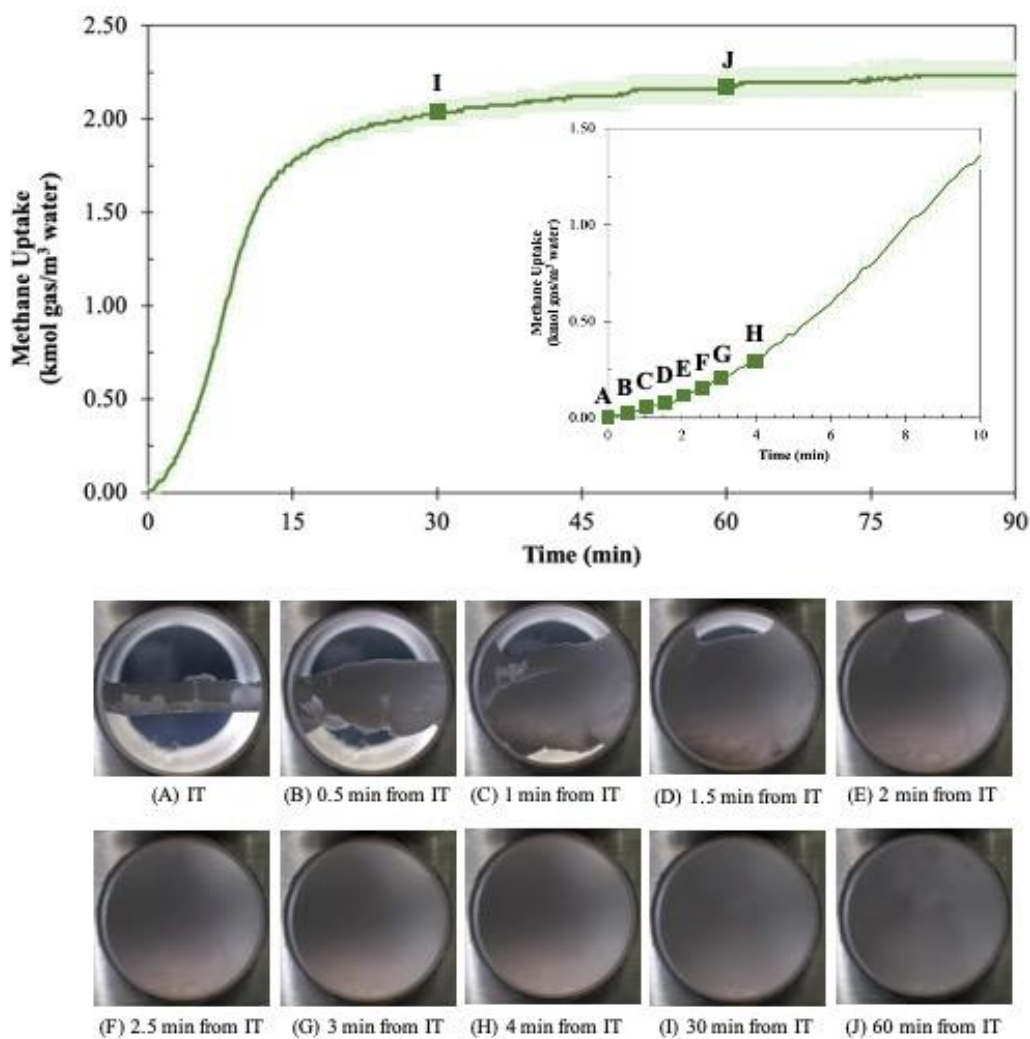


**Figure 4.3** Average methane uptake profile of mixed methane-pyrrolidine hydrates (P1 – P3 experiments) together with the visual observations for an experimental trial P1.

The average methane uptake profile along with the visual observations of mixed methane-pyrrolidine hydrates at 8 MPa and 285.2 K is presented in Figure 4.3. The methane uptake here is plotted only for the hydrate growth phase. Any gas uptake before this phase such as dissolution state is not considered and is removed. And the time zero is referred to the start of the hydrate nucleation, or it can be stated that it corresponds to the hydrate induction time. The shaded-highlight region in this figure represents the standard deviation during the hydrate formation (from at least 3 experiments). According to Figure 4.3 and Table 4.2, the rapid hydrate growth with the hydrate formation rate of  $8.4376 \pm 0.1260$  kmol/hr/m<sup>3</sup> is achieved. This super-fast

rate leads to the completion of hydrate formation within only 80 minutes and also substantiates the fact that pyrrolidine and water molecules have an attractive intermolecular force, which could enhance the hydrate formation rate. There is no substantial change in the slope of methane uptake profile after this time interval, and the methane uptake of  $2.4784 \pm 0.0687$  kmol/m<sup>3</sup> is obtained. The morphology during the formation of mixed methane-pyrrolidine hydrates is presented in Figures 4.3A–J. This morphology observation belongs to the P1 experiment, and it should be noted that the morphology observation and methane uptake are consistent for all separate experiments, as seen by the small shaded-highlight region in Figure 4.3. Therefore, the use of P1 experiment morphology is reasonable to explain the average methane uptake profile. It can be seen that the hydrate nucleation occurs at the gas-liquid interface, as shown in Figure 4.3A. This is due to the highest contact area between the gas and liquid phases, so that the gas molecules have enough area to dissolve into the solution. Thereafter, the hydrates rapidly grow along the crystallizer wall in both upward direction to the gas phase and the downward direction to the bulk solution (Figures 4.3B–E). After 2.5 minutes from the nucleation, the hydrates fully cover the entire crystallizer window (Figure 4.3F), although the corresponding methane uptake is only 0.19 kmol/m<sup>3</sup> (7.7 % of total methane uptake). This behavior can be explained by the two-step hydrate growth mechanism, which was also mentioned in the systems with THF (Kumar *et al.*, 2016; Veluswamy *et al.*, 2016c). This mechanism was well explained by Seo *et al.* (2009), who employed the in-situ Raman spectroscopy for molecular level study. They documented that significant THF encapsulation in the large cages initially occurred during the hydrate growth after nucleation, followed by the enclathration of methane into the small cages of sII hydrates. In the same way, it is thereby reasonable to postulate that pyrrolidine preferentially occupies the large cages in the first step, and the subsequent rapid methane encapsulation emerges in the second step, resulting in the significant increase in the gas uptake. This is obviously shown in the methane uptake profile, while there is no significant change in the visual observation (Figures 4.3G–J). However, at 30 minutes after the nucleation, the thickness of the hydrates can be observed through an increase in the opacity at the corner of the crystallizer window (Figure 4.3I) implying that the continuous hydrate



3243175980

CU IThesis 6271006063 thesis / rev: 19072564 14:31:51 / seq: 40



growth may occur inside the crystallizer and could not be clearly seen by this crystallizer.

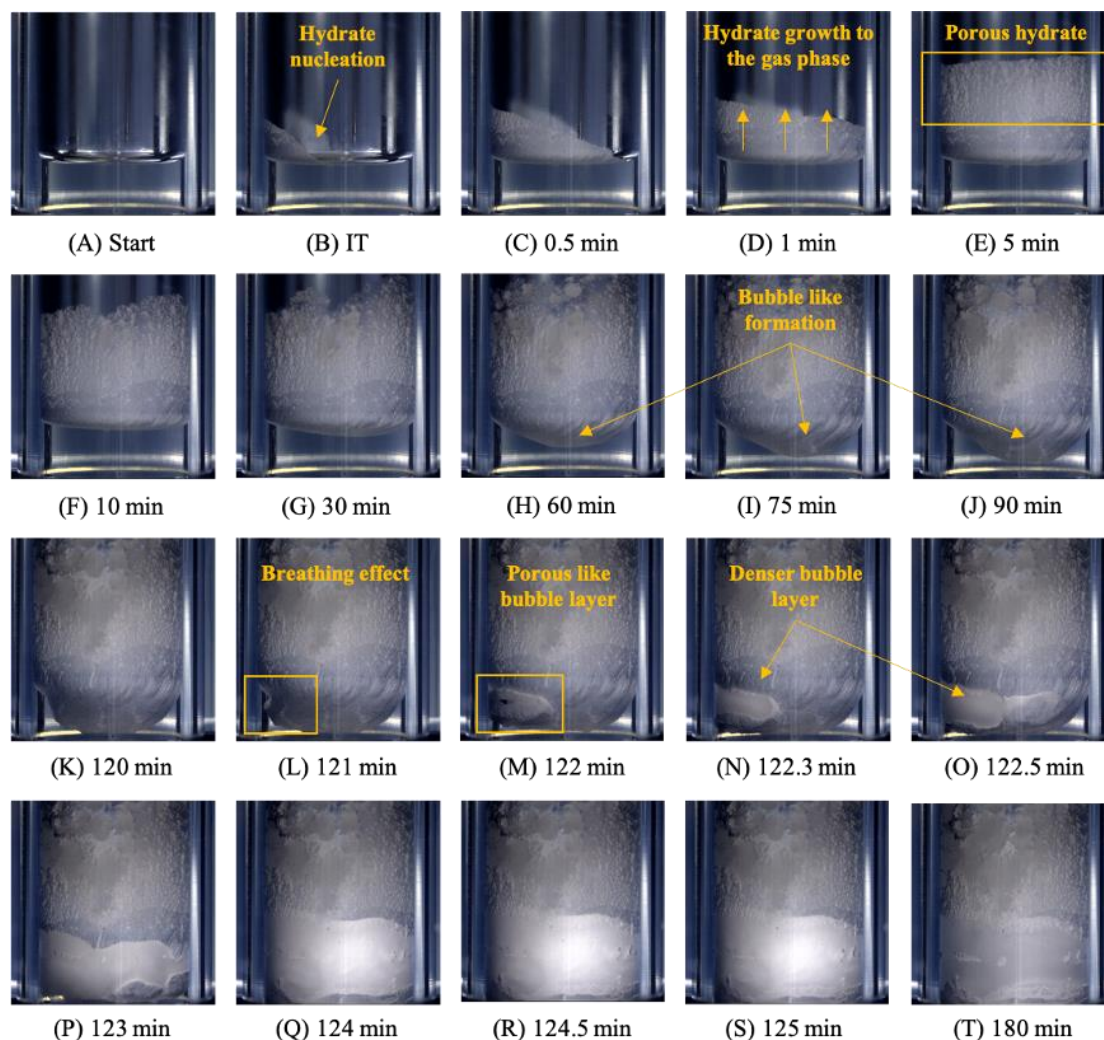


**Figure 4.4** Morphological observation of methane hydrate formation using 5.56 mol% pyrrolidine as a promoter at 8 MPa and 285.2 K in the sapphire crystallizer.

In order to better observe the morphology of hydrate growth of mixed methane-pyrrolidine hydrates, a formation experiment was considered at the same experimental condition as above (285.2 K and 8 MPa) in a sapphire crystallizer. This sapphire crystallizer has a smaller volume and smaller contact area between the gas and liquid phases. The rate of hydrate formation was expected to be slower than that of the previous crystallizer, allowing for clear observation. Figure 4.4 presents a series of morphological observations during the hydrate nucleation and growth at selected

time intervals. Noted that this experiment was performed just to observe the morphology, so the kinetic data including IT, NR<sub>15</sub>, t<sub>90</sub>, and methane uptake were not recorded for this experiment. At the start of the experiment, both gas and liquid phases are clearly separated, as shown in Figure 4.4A. As mentioned earlier, the hydrate nucleation occurs at the gas-liquid interface at the induction time (Figure 4.4B). After the nucleation, it can be observed that the hydrates first grow in the upward direction to the gas phase along the crystallizer wall (Figure 4.4C). Furthermore, the crater-like formation is initiated with continuously growing hydrates in the upward direction after 1 minute from the induction time (Figures 4.4D–F). Besides, the hydrates formed at these intervals are porous. This phenomenon corresponds with the report of Veluswamy *et al.* (2016c). They reported that the capillary suction of the solution towards the crystallizer surface might be the reason. Moreover, as the solution migrates from the bulk solution through the capillary action via the interstitial porous channels, it facilitates the continuous renewal of the gas-liquid interface at the crystallizer wall causing the uninterrupted hydrate growth in the upward direction. Thereafter, it can be seen that the hydrates start to grow downward into the bulk solution with ‘bubble-like’ formation. The methane bubbles gradually increase its size over a period of time (Figures 4.4G–J). This characteristic growth was also investigated in the morphology study of methane hydrate formation in the presence of L-leucine (Veluswamy *et al.*, 2016a). However, the reason for this behavior has not yet been fully explained. After the nucleation at t = 120 minutes, the methane bubbles reach the bottom and start expanding from the backside of the crystallizer together with the first appearance of ‘breathing effect’ (Figures 4.4K–L). Following this, the rapid bubble-like growth is observed (Figures 4.4M–O). It is clearly seen from Figure 4.4M that the hydrates inside the bubble are initially porous like structure before they turn dense in Figures 4.4N–O. This phenomenon indicates the connected channel between the parent hydrate layer and the growing bubble hydrate layer, which acts as a bridge for the gas molecules above the hydrate layer to interact with the bulk solution, resulting in an additional conversion of water to hydrates (Veluswamy *et al.*, 2016a). Thereafter, the thickening process expands throughout the bulk solution (Figures 4.4P–S). This continuous process continues until 180 minutes from the induction time (Figure 4.4T), and no further significant



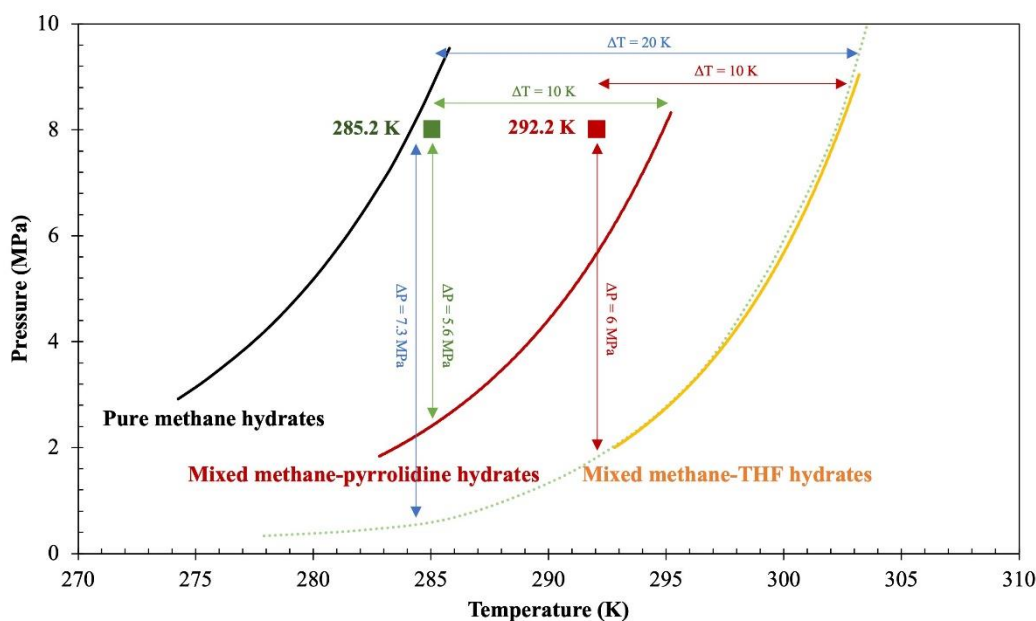
3243175980

CU IThesis 6271006063 thesis / rev: 19072564 14:31:51 / seq: 40

difference in the hydrate formation progress can be observed from this point of time. The morphological observation here enables us to further understand the hydrate formation mechanism using pyrrolidine as a promoter. The methane bubble and breathing effect may occur from an amino functional group since it shows exactly similar pattern with amino acid (L-leucine) even though pyrrolidine and L-leucine have totally different structures (Veluswamy *et al.*, 2016a).

#### 4.2.2 Effects of the Same Driving Force and the Same Experimental Condition on the Mixed Methane-pyrrolidine and Mixed Methane-THF Hydrate Formation

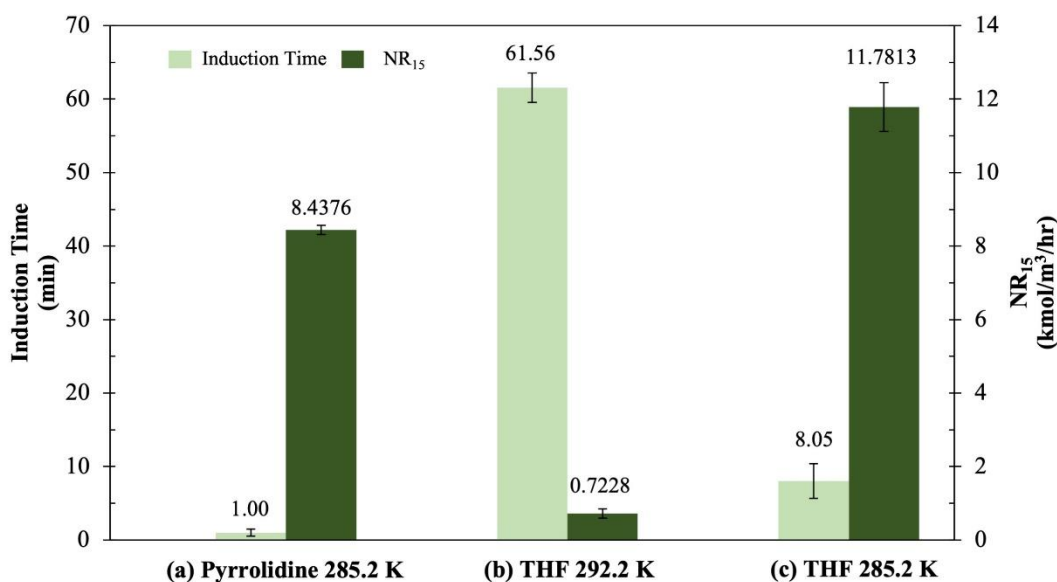
As mentioned in the previous section, the mixed methane-pyrrolidine hydrates are sII. Similarly, THF is one of the well-known promoters forming the same structure (Inkong *et al.*, 2019; Veluswamy *et al.*, 2016c). They reported that THF performed very well in both thermodynamic and kinetic improvement. Hence, to compare the kinetic improvement ability with this promoter, the experiments using THF and pyrrolidine were kinetically compared. Initially, the effects of the same driving force using 5.56 mol% are discussed followed by the discussion on the effects of the same experimental condition on the methane hydrate formation. For the same driving force, the conditions for the mixed methane-pyrrolidine and mixed methane-THF hydrate systems are at the same pressure of 8 MPa but with different temperatures of 285.2 and 292.2 K, respectively. According to Figure 4.5, both systems have an identical temperature driving force of ~10 K and a very close pressure driving force of ~5.6 MPa for the mixed methane-pyrrolidine hydrates and ~6 MPa for the mixed methane-THF hydrates. For the same condition, both systems were carried out at 8 MPa and 285.2 K. At this condition, the mixed methane-THF hydrate system has much higher driving force in both temperature and pressure, ~20 K and ~7.3 MPa, respectively, than those of the mixed methane-pyrrolidine hydrate system, which has the driving force of only ~10 K and ~5.6 MPa. Again, each experiment in this study was repeated at least three times in order to ensure the reproducibility.



**Figure 4.5** Temperature and pressure driving forces of the experiments at 285.2 and 292.2 K and 8 MPa of both methane-pyrrolidine and methane-THF hydrate system.

From the results shown in Table 4.2 and Figure 4.6, it is evident that under the same driving force, pyrrolidine gives much faster induction time about 60 times than THF, indicating a shorter waiting time for the nucleation of the mixed methane-pyrrolidine hydrates. As claimed, pyrrolidine can act as both hydrogen bond donor and acceptor, while THF acts only as a hydrogen bond acceptor. As a result, THF is able to form the hydrogen bond with water through its oxygen atom only (Liu *et al.*, 2019; Shultz and Vu, 2015), whereas pyrrolidine can do likewise through its both nitrogen and hydrogen atoms. It might be due to this reason that THF does not have the ability to promote the nucleation at the beginning of the process as compared to pyrrolidine. Besides the induction time, Figure 4.6 also presents  $NR_{15}$  of both mixed methane-pyrrolidine and mixed methane-THF hydrates. It can be seen that pyrrolidine is excellent in terms of the rate of hydrate formation under the same driving force, as  $NR_{15}$  of the mixed methane-pyrrolidine system is ten times higher than that of the mixed methane-THF system ( $8.4376 \pm 0.1260 \text{ kmol/hr/m}^3$  and  $0.7228 \pm 0.1252 \text{ kmol/hr/m}^3$ , respectively). Inkong *et al.* (2019) and Jeenuang *et al.* (2021) reported that it was impossible for only 5.56 mol% THF to give a rapid rate of hydrate formation at this driving force. They performed the experiments at 8 MPa and 293.2

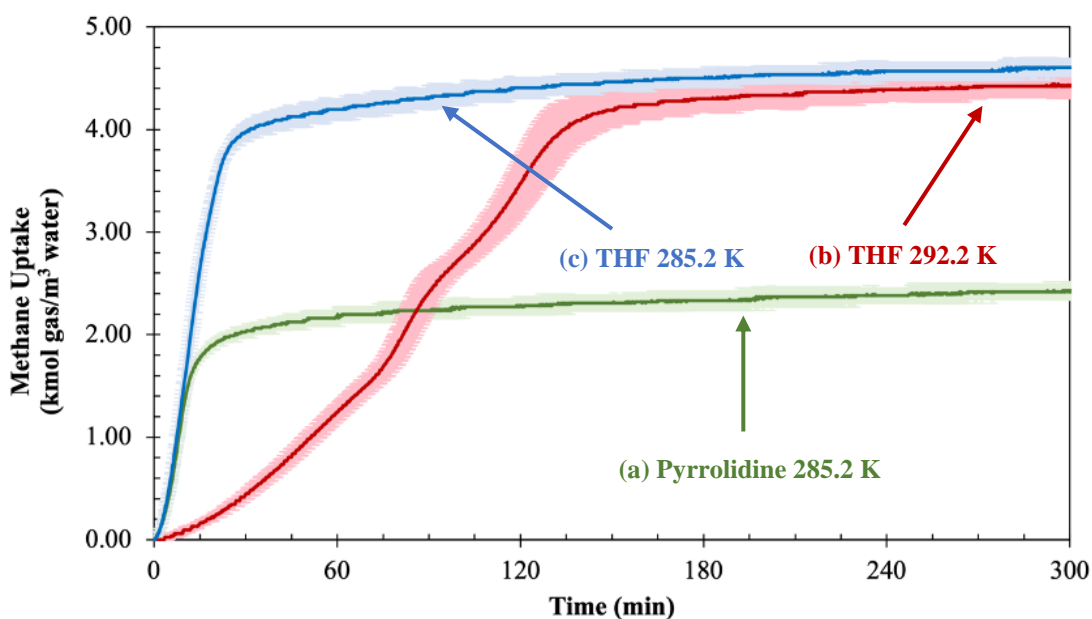
K using THF as a promoter (almost the same driving force with the pyrrolidine system in this study) and informed that a co-promoter such as an amino acid or a surfactant was necessary in order to achieve the rapid hydrate formation rate. Remarkably, thanks to the kinetic improvement of pyrrolidine, this very fast rate is obtained using only pyrrolidine without any co-promoter. This result confirms the assumption that pyrrolidine can act as a thermodynamic and kinetic promoter at the same time. These interesting results, IT and  $NR_{15}$ , may be due to the combination of functions between THF and amino acids as pyrrolidine has an analogous structure and has an amino functional group.



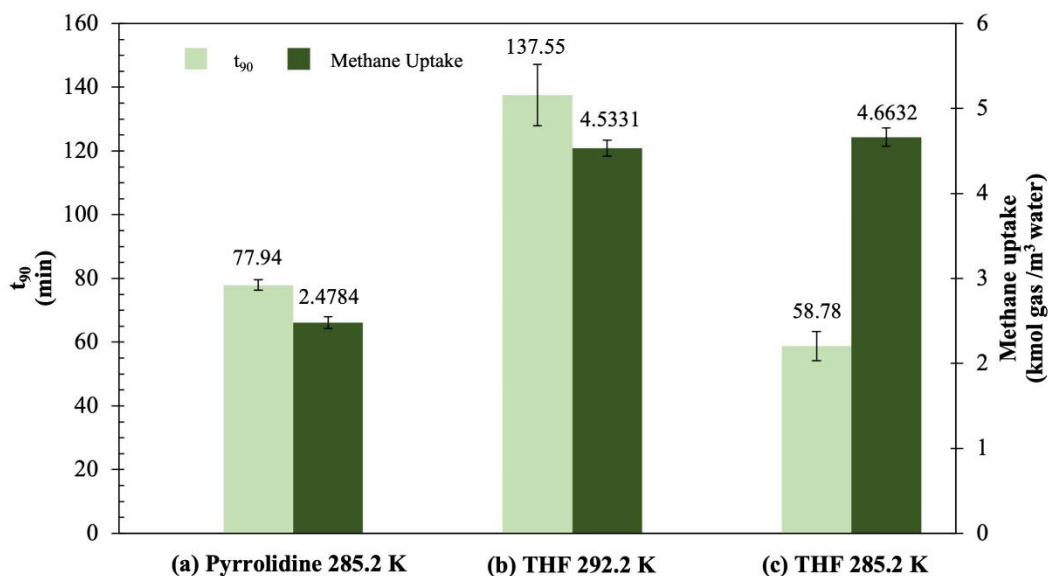
**Figure 4.6** Comparison of the induction time (IT) and the normalized rate of hydrate formation ( $NR_{15}$ ) with different promoters at the same driving force ((a) and (b)) and the same experimental condition ((a) and (c)).

Figure 4.7 compares the methane uptake profiles for the mixed methane-pyrrolidine and mixed methane-THF systems. Under the same driving force, it is manifest from line (a) and (b) that the slope of the mixed methane-pyrrolidine system is much steeper, confirming a very fast rate of hydrate formation. Consequently, it can be observed that the hydrate growth almost completes within 80 minutes for pyrrolidine experiments, while it takes about 140 minutes for THF experiments. These durations are called  $t_{90}$ , indicating the time that reaches 90% of total methane

uptake, and are also shown in Figure 4.8. In terms of methane consumption, THF outperforms pyrrolidine by approximately two times. THF gives higher methane consumption of  $4.5331 \pm 0.0956 \text{ kmol/m}^3$ , whereas it is only  $2.4784 \pm 0.0687 \text{ kmol/m}^3$  for pyrrolidine, as shown in Figure 4.8. This methane uptake value of the mixed methane-pyrrolidine system is not what was expected. The exact reason for lower methane uptake with pyrrolidine has not clearly been reported. However, based on this study, it might be due to the intermolecular force, which is the hydrogen bond, as mentioned earlier. Although it is beneficial for the induction time and the rate of hydrate formation, it would result in lower methane uptake. However, the investigation in the molecular level is required to substantiate this explanation.



**Figure 4.7** Average methane uptake profiles from methane hydrate formation with different promoters at the same driving force (line (a) and (b)) and the same experimental condition (line (a) and (c)).



**Figure 4.8** Comparison of the average time to reach 90% of methane uptake ( $t_{90}$ ) and the average final methane uptake with different promoters at the same driving force ((a) and (b)) and the same experimental condition ((a) and (c)).

In order to analyze in another perspective, the comparison of mixed methane-pyrrolidine and methane-THF formation was also carried out at the same condition. Figures 4.6a and 4.6c show the induction time and  $NR_{15}$  of both systems under the same condition. The result shows that even though the mixed methane-pyrrolidine system has much lower driving force in both temperature and pressure, it still gives almost eight times faster induction time of only  $1.00 \pm 0.50$  minute compared to  $8.05 \pm 2.36$  minutes of the mixed methane-THF system. This evidently reconfirms the previous explanation that the additional hydrogen-bond sites of pyrrolidine may have the capability to promote the mixed methane hydrate nucleation. For this reason, it might also be stated that this hydrogen bonding between pyrrolidine and water has a greater impact on the hydrate nucleation than the driving force. Moreover, it can be seen that the  $NR_{15}$  in the mixed methane-THF system is approximately 30% higher than that in the mixed methane-pyrrolidine system. This is strongly attributed to the much higher driving force for the mixed methane-THF system. The driving force is like the force pushing methane molecules to be captured in the small cages. The higher the driving force the system has, the higher the rate of hydrate formation is achieved, allowing a rapid and sustaining hydrate formation

(Bhattacharjee *et al.*, 2020). Due to the faster rate of hydrate formation obtained from the mixed methane-THF system, the 90% completion of hydrate formation for this system is also faster than that of the pyrrolidine system ( $58.78 \pm 4.60$  and  $77.94 \pm 1.59$  minutes, respectively), as shown in Figures 4.8a and 4.8c). However, it is interesting to note that the slope of the gas uptake profiles in both systems during the first 10 minutes of the experiment under the same condition, line (a) and (c) in Figure 4.7, are almost overlapped. This is surprising as pyrrolidine can enhance the formation rate to close to that of the mixed methane-THF system in the first 10 minutes albeit the much lower driving force of the pyrrolidine system. At the end of the experiment at the similar condition, THF provides higher methane uptake than pyrrolidine ( $4.6632 \pm 0.1080$  and  $2.4784 \pm 0.0687$  kmol/m<sup>3</sup>, respectively). It is also clear that the final methane uptakes of the mixed methane-THF system at both conditions are not significantly different. This corresponds to the result by Veluswamy *et al.* (2016b), who reported that the temperature did not affect the final methane uptake of mixed methane-THF hydrates.

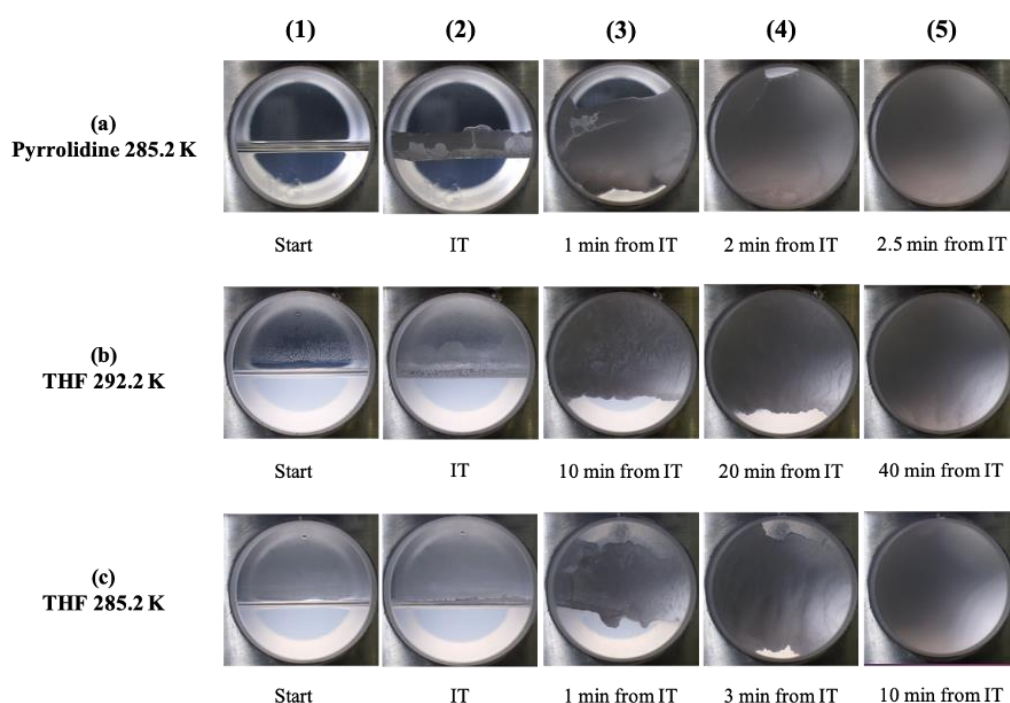


**Figure 4.9** Morphology observations of P1, T1, and T5 trials during the methane hydrate formation in the presence of (a) pyrrolidine at 285.2 K, (b) THF at 292.2 K, and (c) THF at 285.2 K.



The visual observations of mixed methane-THF and mixed methane-pyrrolidine hydrate formation of both under the same driving force and the same condition are presented in Figure 4.9. Figures 4.9 (a1), (b1), and (c1) demonstrate that the methane gas and liquid phases stay separately inside the crystallizer at the beginning. Then, all systems even at different conditions show the same behavior that the hydrates first occur at the gas-liquid interface, as shown in Figures 4.9 (a2), (b2), and (c2). After that, the hydrates in all systems continuously grow in both upward and downward directions to the gas and liquid phases, respectively. For the systems under the same driving force, Figures 4.9 (a3–a5) indicate that the mixed methane-pyrrolidine hydrates form very rapidly until there is no significant change after only 2.5 minutes from the nucleation, whereas the mixed methane-THF system takes much longer, 40 minutes, Figures 4.9 (b3–b5). This duration corresponds with the fast rate of hydrate formation using pyrrolidine. Moreover, it can be seen that the difference between these two promoters is that the mixed methane-THF hydrates first grow upward and then expand downward, whereas the mixed methane-pyrrolidine hydrates simultaneously grow upward and downward. For the system under the similar conditions, Figures 4.9 (c3–c5) show that there is no significant difference until 10 minutes after the hydrate nucleation for the mixed methane-THF hydrate system. One may wonder why it takes longer in spite of the fact that THF gives higher rate of hydrate formation at this condition than that of pyrrolidine. The answer might be due to the fact that the morphology in Figure 4.9 only shows the hydrate formation at the crystallizer wall with a limited viewpoint, therefore, the formation cannot be thoroughly observed. The hydrates might grow densely inside the crystallizer before going toward the wall, resulting in the longer time. In addition, in the previous section, the two-step hydrate growth mechanism can be seen in the mixed methane-pyrrolidine system. Interestingly, the same phenomenon can also be found in the mixed methane-THF system implying that both promoters have the same behavior. To confirm this, Figures 4.9b5 and 4.9c5 show that the hydrates fill the entire crystallizer window despite the methane uptakes for both systems at this time are  $0.6860 \text{ kmol/m}^3$  (12.4 % from the total methane uptake) and  $1.5620 \text{ kmol/m}^3$  (33.5 % from the total methane uptake), respectively. This confirms that the promoters first occupy the large

cages, followed by the encapsulation of methane gas molecules into the small cages of sII hydrates (Kumar *et al.*, 2016).

#### 4.2.3 Mixed Methane-THF and Mixed Methane-pyrrolidine Hydrate Dissociation

As mentioned in the experimental section, the dissociation experiments were performed after the completion of hydrate formation in order to comprehend the decomposition behavior. The hydrates were dissociated using a simple thermal stimulation technique. The temperature inside the crystallizer was increased to 308.2 K, which is out of the stable zone of the phase equilibrium line for both promoters. From the results, shown in Table 4.2 and Figure B4, the methane gas is almost completely recovered. The final gas recovery for all experiments is in the range of 95–98 %, which is very beneficial for SNG commercialization. In order to further demonstrate the dissociation process in terms of kinetics, Figure 4.10 presents the average normalized gas recovery. It should be emphasized that the mixed methane-pyrrolidine and mixed methane-THF systems in the green and red lines, respectively, are not in the similar formation condition, but they are at the same driving force. Thus, they are comparable in terms of hydrate stability under the same heating rate of the dissociation process. Obviously, after around 30 minutes from the beginning of the dissociation, the mixed methane-THF system starts to decompose, whereas it takes approximately 35 minutes for the mixed methane-pyrrolidine system. This implies that the mixed methane-pyrrolidine hydrates are more stable than the other since they need more heat to start the melting process. This might be due to the hydrogen bond between pyrrolidine and water. This bond may hold pyrrolidine and water together, resulting in the strength of the hydrate structure. After the sufficient heat is provided, the hydrates begin to melt, and the trapped methane gas molecules are released from the small cages of sII hydrates. Though the mixed methane-THF hydrates start to melt first, they store more gas molecules in their structure, resulting in a little longer time to complete the process. Remarkably, initially, the hump is observed due to the thermal expansion of remaining methane gas in the gas phase. On the other hand, the mixed methane-THF hydrates in the blue line take the longest time, approximately 50 minutes, to begin to melt. According to the phase equilibrium,



3243175980

CU Theses 6271006063 thesis / recv: 19072564 14:31:51 / seq: 40

shown in Figure 4.5, the system in the blue line has the highest driving force for the formation. Consequently, the highest energy is also required for decomposition.

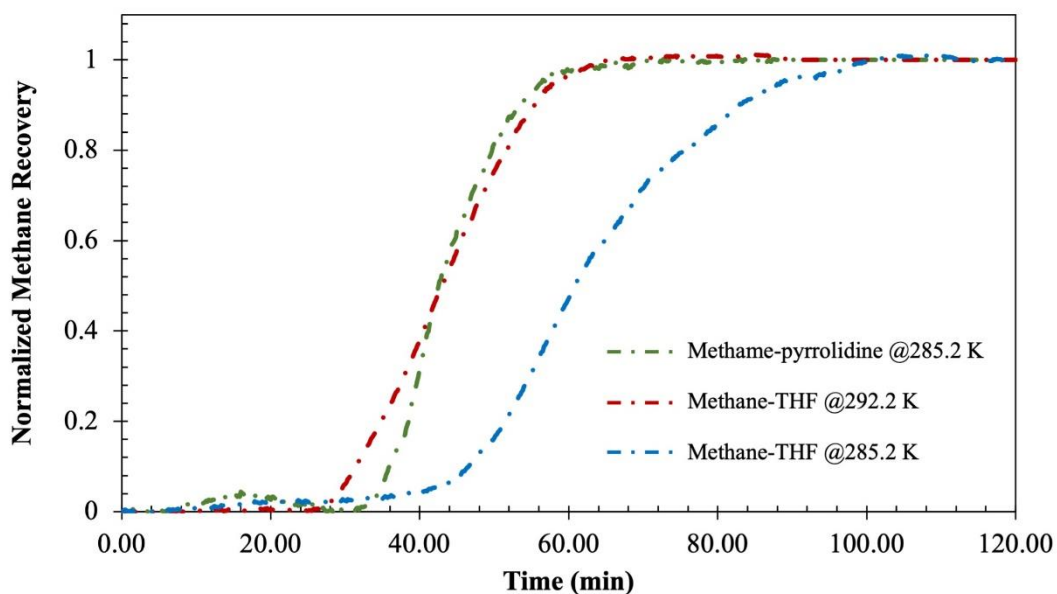


**Figure 4.10** Average normalized methane recovery during the decomposition process in the presence of different promoters under different initial conditions.

To map with the normalized methane recovery, Figure 4.11 presents the morphology of the experiments with different promoters during the dissociation process. The beginnings of all dissociation experiments start from the window, then throughout the core of the crystallizer. This is due to the fact that the crystallizer is surrounded with heating water, as shown in the schematic apparatus (Figure 3.1). For the mixed methane-pyrrolidine hydrates, Figure 4.11a, it can be observed that the hydrates begin to dissociate after 34 minutes from the start of the process. At 45 minutes from the start, the methane gas bubbles can be seen since the gas molecules are released out from the small cages of sII hydrates. It takes about 70 minutes for the hydrates in this system to completely decompose. The system then is back to the origin of the process, which is the separation between methane gas and liquid bulk solution. Figures 4.11b and 4.11c present the morphology of the dissociation of the mixed methane-THF hydrates at the same driving force and the same condition for the formation with the previous system, respectively. For the system at the same driving

force, the liquid droplets at the crystallizer window are observed after only 30 minutes from the start. Thereafter, the system continues to decompose until the completion at around 70 minutes. This observation emphasizes the stability of the mixed methane-pyrrolidine hydrates compared to the mixed methane-THF hydrates. For the system at the similar condition, it takes longer for the hydrates to decompose and to complete the process (50 minutes and 100 minutes, respectively). This is due to the highest driving force of the system, as already mentioned earlier. These morphological observations are related with the normalized methane gas recovery in Figure 4.10. Moreover, it was reported that there was foam formation at the end of the decomposition process of mixed methane hydrates in the presence of surfactant (Pandey *et al.*, 2018; Viriyakul *et al.*, 2021). Fortunately, both mixed methane-pyrrolidine and mixed methane-THF hydrates do not generate foam, which is preferable for large scale natural gas storage and transportation. The present outcomes enable the discovery of more precise backgrounds to pick the best promoters and can be extended to forecast the most suitable properties of chemicals for the use in clathrate hydrates and SNG technology in the future.

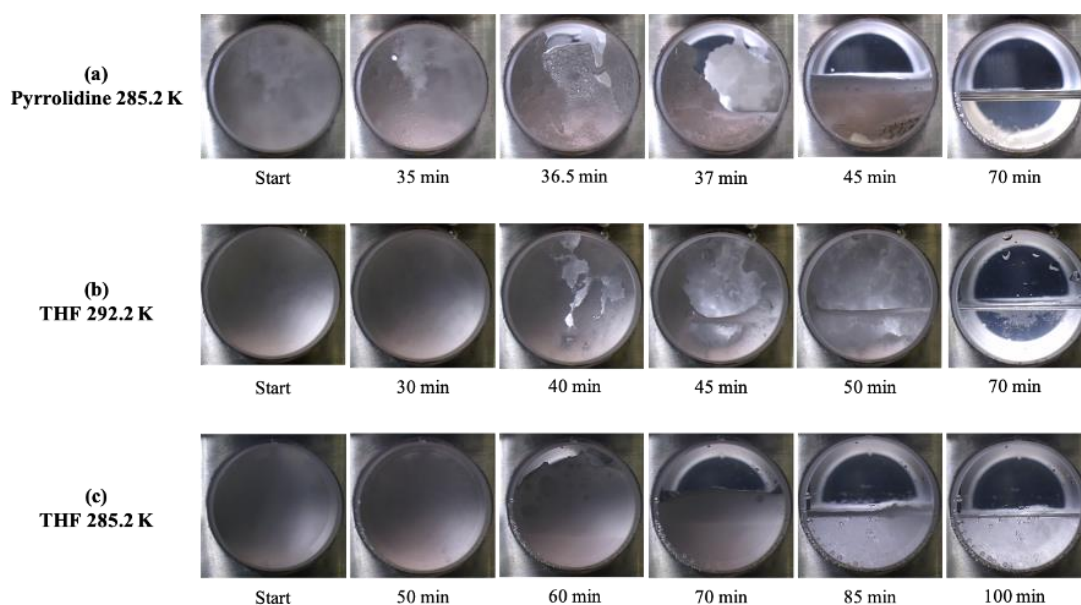


**Figure 4.11** Morphology observations of P1, T2 and T5 trials during the decomposition process in the presence of different promoters.

## CHAPTER 5

### CONCLUSIONS AND RECCOMENDATIONS

#### 5.1 Conclusions

In this work, the thermodynamics, kinetics along with morphology of methane hydrate formation were investigated in the presence of pyrrolidine at the 5.56 mol% stoichiometric ratio. The investigations of pyrrolidine were also compared with those of THF, an outstanding thermodynamic promoter. The results showed that pyrrolidine could be a thermodynamic promoter. Although pyrrolidine cannot thermodynamically promote as well as THF, it can shift the phase equilibrium of pure methane sI hydrates to much milder conditions. In terms of kinetics, the experiments were carried out at the same driving force and the same experimental condition for both pyrrolidine and THF. The results indicated that pyrrolidine could also be a kinetic promoter. Under the same driving force, pyrrolidine alone could give the rate of hydrate formation almost equivalent to that obtained from the synergism of THF and amino acids. Besides, all kinetic data including the IT, NR<sub>15</sub>, and t<sub>90</sub> were better compared to those of THF, except the final methane uptake which was lower. This might be owing to the hydrogen bond between pyrrolidine and water. However, under the same experimental condition, THF outperformed pyrrolidine in almost all kinetic aspects since it had more driving force at the beginning of the process. Interestingly, the morphology experiment presented that the hydrate formation using pyrrolidine as a promoter showed similar unique characteristic with L-leucine amino acid, which was beneficial for the hydrate formation rate.

#### 5.2 Recommendations

To confirm the explanations in this research and obtain further understanding about the effects of using pyrrolidine as a promoter, especially on the formation kinetics, the molecular level study, such as in-situ Raman spectroscopy and density-functional theory (DFT) computation, needs to be investigated. Moreover, in order to

explain more about the exclusive phenomena of pyrrolidine in this research, i.e., further pressure drop and single nucleation during the thermodynamic study, more experiments need to be considered.

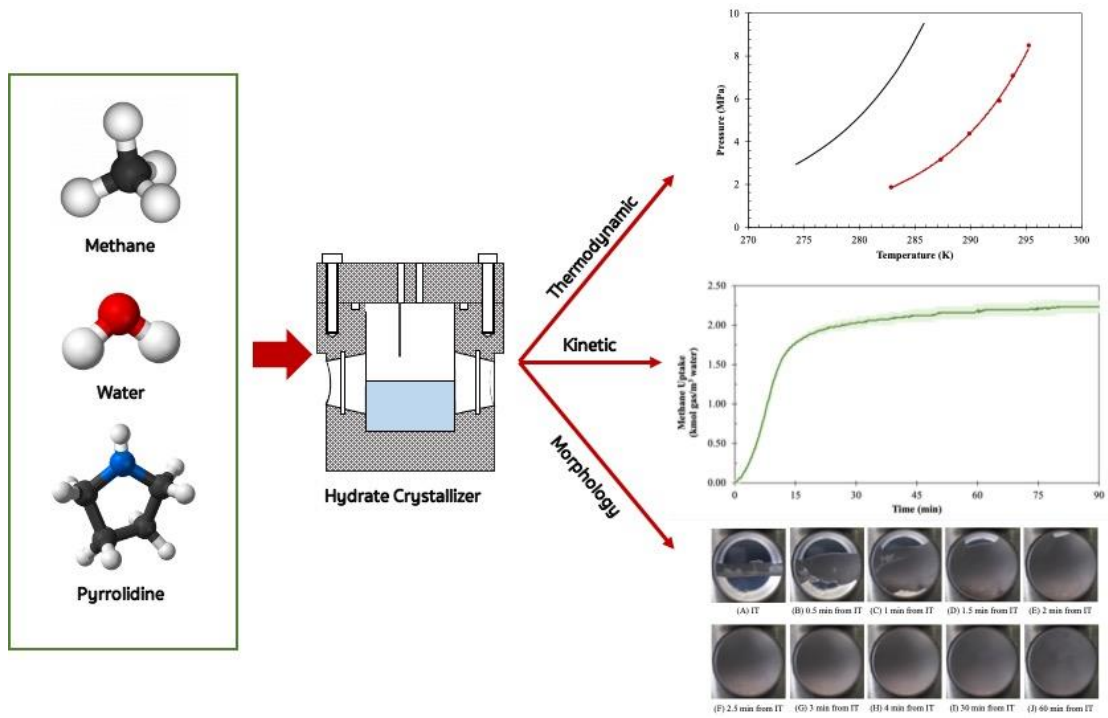


3243175980

CU IThesis 6271006063 thesis / recv: 19072564 14:31:51 / seq: 40

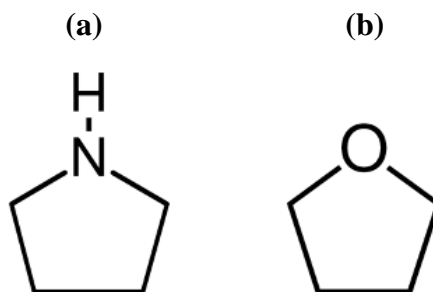
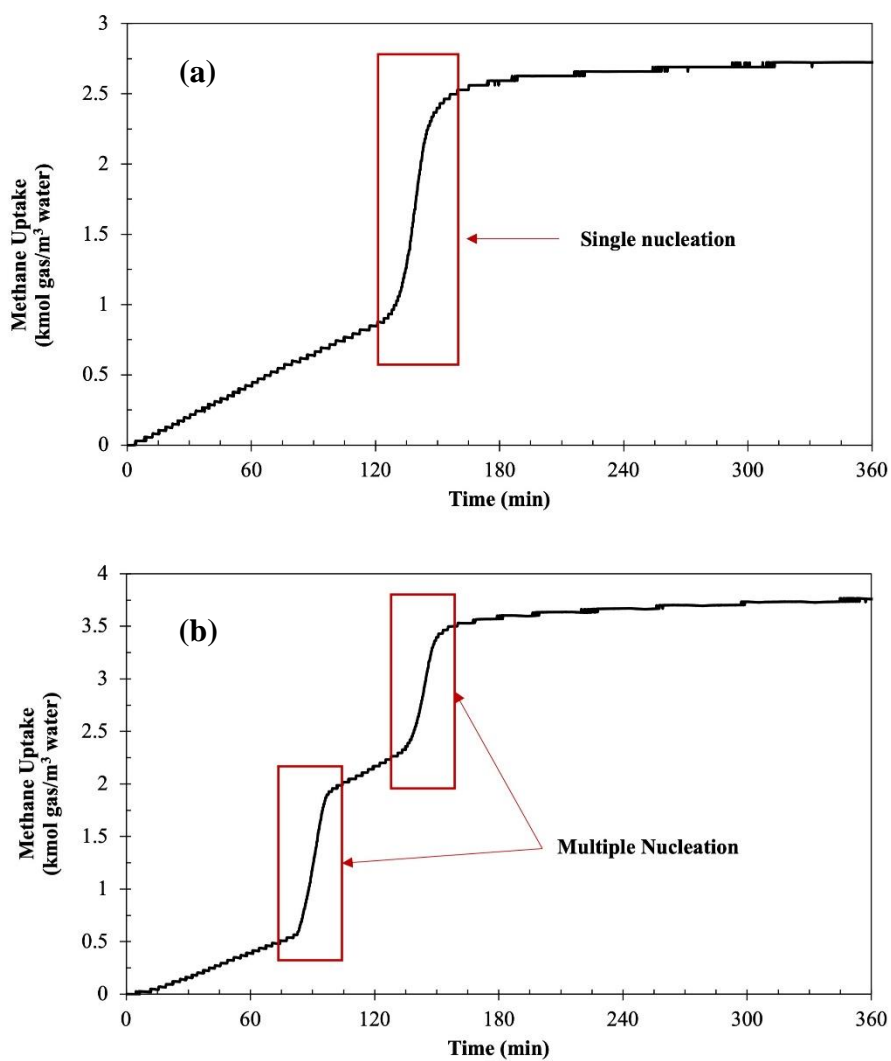
# APPENDICES

## Appendix A Graphical Abstract



**Figure A1** Schematic of the mixed methane hydrate formation using pyrrolidine as a hydrate promoter together with the summary results of thermodynamics, kinetics, and morphology.

## Appendix B Supporting Information

**Figure B1** Chemical structure of (a) Pyrrolidine and (b) THF.**Figure B2** Methane uptake profiles during thermodynamic studies using (a) 5.56 mol% pyrrolidine and (b) 5.56 mol% THF as a promoter at 4.5 MPa.



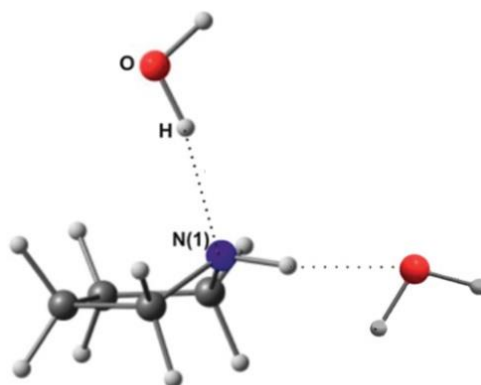


**Figure B3** Simulated hydrogen bonding between pyrrolidine and water molecule, presenting a capability of hydrogen bond donor and acceptor (Modified from (Marczak *et al.*, 2017).

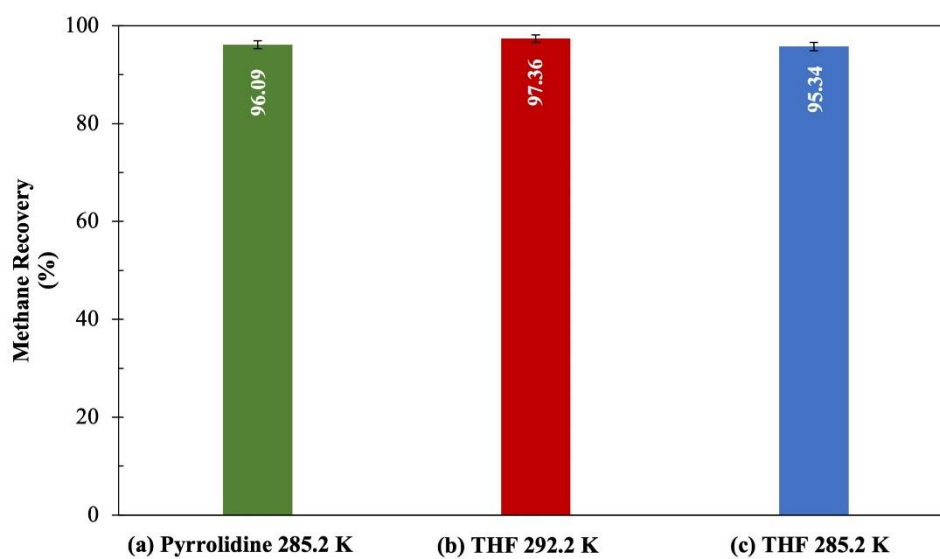


**Figure B4** Average methane recovery with standard error after methane hydrate dissociation using pyrrolidine and THF as a promoter.

## REFERENCES

- Aman, Z. M., and Koh, C. A. (2016). Interfacial phenomena in gas hydrate systems. Chemical Society Reviews, 45(6), 1678-1690.
- Arora, A., Cameotra, S. S., and Balomajumder, C. (2015). Natural Gas Hydrate as an Upcoming Resource of Energy. Journal of Petroleum & Environmental Biotechnology, 6.
- Asadi, F., Metaxas, P. J., Lim, V. W. S., Nguyen, T. A. H., Aman, Z. M., May, E. F., and Nguyen, A. V. (2020). Cyclodextrins as eco-friendly nucleation promoters for methane hydrate. Chemical Engineering Journal, 127932.
- Bavoh, C. B., Lal, B., Osei, H., Sabil, K. M., and Mukhtar, H. (2019). A review on the role of amino acids in gas hydrate inhibition, CO<sub>2</sub> capture and sequestration, and natural gas storage. Journal of Natural Gas Science and Engineering, 64, 52-71.
- Bavoh, C. B., Nashed, O., Khan, M. S., Partoon, B., Lal, B., and Sharif, A. M. (2018). The impact of amino acids on methane hydrate phase boundary and formation kinetics. The Journal of Chemical Thermodynamics, 117, 48-53.
- Beheshtimaal, A., and Haghtalab, A. (2018). Thermodynamic modeling of hydrate formation conditions using different activity coefficient models in the presence of tetrahydrofuran (THF). Chemical Engineering Research and Design, 129, 150-159.
- Bhattacharjee, G., Prakash Veluswamy, H., Kumar, R., and Linga, P. (2020). Rapid methane storage via sII hydrates at ambient temperature. Applied Energy, 269, 115142.
- C2ES. (2013). Leveraging Natural Gas to Reduce Greenhouse Gas Emissions. Arlington, VA 22201: Center for Climate and Energy Solutions.
- Chang, K.-Y., Chu, C.-K., Chu, L.-S., Chen, Y.-A., Lin, S.-T., Chen, Y.-P., and Chen, L.-J. (2020). Effect of Small Cage Guests on Dissociation Properties of Tetrahydrofuran Hydrates. The Journal of Physical Chemistry B, 124(33), 7217-7228.
- Davy, H. (1811). VIII. On a combination of oxymuriatic gas and oxygene gas. Philosophical Transactions of the Royal Society of London, 101, 155-162.
- Demirbas, A. (2010). Methane Gas Hydrate. London: Springer.

- Dobrzycki, L., Taraszewska, P., Boese, R., and Cyrański, M. K. (2015). Pyrrolidine and Its Hydrates in the Solid State. Crystal Growth & Design, 15(10), 4804-4812.
- EIA. (2020). Annual Energy Outlook 2020 with projections to 2050. U.S. Department of Energy Washington, DC 20585: U.S. Energy Information Administration.
- Englezos, P. (1993). Clathrate hydrates. Industrial & Engineering Chemistry Research, 32(7), 1251-1274.
- Englezos, P., Kalogerakis, N., Dholabhai, P. D., and Bishnoi, P. R. (1987). Kinetics of formation of methane and ethane gas hydrates. Chemical Engineering Science, 42(11), 2647-2658.
- Ganji, H., Manteghian, M., Sadaghiani zadeh, K., Omidkhah, M. R., and Rahimi Mofrad, H. (2007). Effect of different surfactants on methane hydrate formation rate, stability and storage capacity. Fuel, 86(3), 434-441.
- Gómez-Díaz, D., and Navaza, J. M. (2004). Surface Behavior of Aqueous Solutions of Pyrrolidine and Piperidine. Journal of Chemical & Engineering Data, 49(5), 1406-1409.
- Gough, S. R., and Davidson, D. W. (1971). Composition of Tetrahydrofuran Hydrate and the Effect of Pressure on the Decomposition. Canadian Journal of Chemistry, 49(16), 2691-2699.
- Hao, W., Wang, J., Fan, S., and Hao, W. (2008). Evaluation and analysis method for natural gas hydrate storage and transportation processes. Energy Conversion and Management, 49(10), 2546-2553.
- Inkong, K., Rangsunvigit, P., Kulprathipanja, S., and Linga, P. (2019). Effects of temperature and pressure on the methane hydrate formation with the presence of tetrahydrofuran (THF) as a promoter in an unstirred tank reactor. Fuel, 255, 115705.
- Jeenmuang, K., Viriyakul, C., Inkong, K., Prakash Veluswamy, H., Kulprathipanja, S., Rangsunvigit, P., and Linga, P. (2021). Enhanced hydrate formation by natural-like hydrophobic side chain amino acids at ambient temperature: A kinetics and morphology investigation. Fuel, 299, 120828.
- Kadam, S. S., Kulkarni, S. A., Coloma Ribera, R., Stankiewicz, A. I., ter Horst, J. H., and Kramer, H. J. M. (2012). A new view on the metastable zone width during

- cooling crystallization. Chemical Engineering Science, 72, 10-19.
- Khurana, M., Yin, Z., and Linga, P. (2017). A Review of Clathrate Hydrate Nucleation. ACS Sustainable Chemistry & Engineering, 5(12), 11176-11203.
- Kumar, A., Daraboina, N., Kumar, R., and Linga, P. (2016). Experimental Investigation To Elucidate Why Tetrahydrofuran Rapidly Promotes Methane Hydrate Formation Kinetics: Applicable to Energy Storage. The Journal of Physical Chemistry C, 120(51), 29062-29068.
- Kumar, A., Veluswamy, H., Kumar, R., and Linga, P. (2019a). Kinetic promotion of mixed methane-THF hydrate by additives: Opportune to energy storage. Energy Procedia, 158, 5287-5292.
- Kumar, A., Veluswamy, H. P., Linga, P., and Kumar, R. (2019b). Molecular level investigations and stability analysis of mixed methane-tetrahydrofuran hydrates: Implications to energy storage. Fuel, 236, 1505-1511.
- Kumar, R., and Linga, P. (2017). Gas Hydrates. In W. M. White (Ed.), Encyclopedia of Geochemistry: A Comprehensive Reference Source on the Chemistry of the Earth (pp. 1-7). Cham: Springer International Publishing.
- Lee, Y.-J., Kawamura, T., Yamamoto, Y., and Yoon, J.-H. (2012). Phase Equilibrium Studies of Tetrahydrofuran (THF) + CH<sub>4</sub>, THF + CO<sub>2</sub>, CH<sub>4</sub> + CO<sub>2</sub>, and THF + CO<sub>2</sub> + CH<sub>4</sub> Hydrates. Journal of Chemical & Engineering Data, 57(12), 3543-3548.
- Liu, J., Yan, Y., Yan, Y., and Zhang, J. (2019). Tetrahydrofuran (THF)-Mediated Structure of THF·(H<sub>2</sub>O)<sub>n=1-10</sub>: A Computational Study on the Formation of the THF Hydrate. Crystals, 9(2).
- Lozano-Castelló, D., Alcañiz-Monge, J., de la Casa-Lillo, M. A., Cazorla-Amorós, D., and Linares-Solano, A. (2002). Advances in the study of methane storage in porous carbonaceous materials. Fuel, 81(14), 1777-1803.
- Luzi, M., Schicks, J. M., Naumann, R., Erzinger, J., Udachin, K. A., Moudrakovski, I. L., Ripmeester, J. A., and Ludwig, R. (2008, July 6-10). Investigations on the Influence of Guest Molecule Characteristics and the Presence of Multicomponent Gas Mixtures on Gas Hydrate Properties. Paper presented at the 6th International Conference on Gas Hydrates (ICGH 2008), Vancouver, British

Columbia, CANADA.

- Marboeuf, U., Schmitt, B., Petit, J.-M., Mousis, O., and Fray, N. (2011, October 01). A model of cometary nucleus taking into account all phase changes of water ice: amorphous, crystalline, and clathrate. Paper presented at the EPSC-DPS Joint Meeting 2011, Nantes, France.
- Marczak, W., Varfolomeev, M. A., Rakipov, I. T., Lodowski, P., Kowalska-Szojda, K., Łęźniak, M., Almásy, L., and Len, A. (2017). Molecular Aggregation in Binary Mixtures of Pyrrolidine, N-Methylpyrrolidine, Piperidine, and N-Methylpiperidine with Water: Thermodynamic, SANS, and Theoretical Studies. The Journal of Physical Chemistry B, 121(14), 3070-3086.
- McCarthy, V. N., and Jordan, K. D. (2006). Structure and stability of the  $(\text{H}_2\text{O})_{21}$  and  $(\text{H}_2\text{O})_{20} \cdot (\text{H}_2\text{S})$  clusters: Relevance of cluster systems to gas hydrate formation. Chemical Physics Letters, 429(1), 166-168.
- Mech, D., and Sangwai, J. S. (2016). Phase Equilibrium of the Methane Hydrate System in the Presence of Mixed Promoters (THF + TBAB) and the Effect of Inhibitors (NaCl, Methanol, and Ethylene Glycol). Journal of Chemical & Engineering Data, 61(10), 3607-3617.
- Nakamura, T., Makino, T., Sugahara, T., and Ohgaki, K. (2003). Stability boundaries of gas hydrates helped by methane—structure-H hydrates of methylcyclohexane and cis-1,2-dimethylcyclohexane. Chemical Engineering Science, 58(2), 269-273.
- Nakane, R., Shimosato, Y., Gima, E., Ohmura, R., Senaha, I., and Yasuda, K. (2021). Phase equilibrium condition measurements in carbon dioxide hydrate forming system coexisting with seawater. The Journal of Chemical Thermodynamics, 152, 106276.
- Pandey, G., Bhattacharjee, G., Veluswamy, H. P., Kumar, R., Sangwai, J. S., and Linga, P. (2018). Alleviation of Foam Formation in a Surfactant Driven Gas Hydrate System: Insights via a Detailed Morphological Study. ACS Applied Energy Materials, 1(12), 6899-6911.
- Papadimitriou, N. I., Tsimpanogiannis, I. N., and Stubos, A. K. (2009). Gas content of binary clathrate hydrates with promoters. The Journal of Chemical Physics,

131(4), 044102.

- Prasad, P. S. R., Sowjanya, Y., and Shiva Prasad, K. (2009). Micro-Raman investigations of mixed gas hydrates. Vibrational Spectroscopy, 50(2), 319-323.
- Ren, Z., Liu, D., Liu, Z., and Pan, Z. (2020). Influence of sodium chloride on the kinetics of methane hydrate formation in the presence of surfactant. Journal of Natural Gas Science and Engineering, 83, 103622.
- Romero Nieto, D., Lindbråthen, A., and Hägg, M.-B. (2017). Effect of Water Interactions on Polyvinylamine at Different pHs for Membrane Gas Separation. ACS Omega, 2(11), 8388-8400.
- Sapag, K., Vallone, A., García Blanco, A., and Solar, C. (2010). Adsorption of Methane in Porous Materials as the Basis for the Storage of Natural Gas. In P. Protocnik (Ed.), Natural Gas (pp. 205-244). New York: InTech.
- Schicks, J. M. (2018). Gas Hydrates: Formation, Structures, and Properties. In H. Wilkes (Ed.), Hydrocarbons, Oils and Lipids: Diversity, Origin, Chemistry and Fate (pp. 1-15). Cham: Springer International Publishing.
- Seo, Y., Lee, J.-W., Kumar, R., Moudrakovski, I. L., Lee, H., and Ripmeester, J. A. (2009). Tuning the Composition of Guest Molecules in Clathrate Hydrates: NMR Identification and Its Significance to Gas Storage. Chemistry – An Asian Journal, 4(8), 1266-1274.
- Shi, L.-L., Liang, D.-Q., and Li, D.-L. (2014). Phase equilibrium conditions for simulated landfill gas hydrate formation in aqueous solutions of tetrabutylammonium nitrate. The Journal of Chemical Thermodynamics, 68, 322-326.
- Shin, W., Park, S., Ro, H., Koh, D.-Y., Seol, J., and Lee, H. (2012). Phase equilibrium measurements and the tuning behavior of new sII clathrate hydrates. The Journal of Chemical Thermodynamics, 44(1), 20-25.
- Shultz, M. J., and Vu, T. H. (2015). Hydrogen Bonding between Water and Tetrahydrofuran Relevant to Clathrate Formation. The Journal of Physical Chemistry B, 119(29), 9167-9172.
- Siangsai, A., Rangsunvigit, P., Kitiyanan, B., Kulprathipanja, S., and Linga, P. (2015). Investigation on the roles of activated carbon particle sizes on methane hydrate

- formation and dissociation. Chemical Engineering Science, 126, 383-389.
- Skovborg, P., and Rasmussen, P. (1994). A mass transport limited model for the growth of methane and ethane gas hydrates. Chemical Engineering Science, 49(8), 1131-1143.
- Sloan, E. D. (2003). Fundamental principles and applications of natural gas hydrates. Nature, 426(6964), 353-359.
- Sloan, E. D., and Koh, C. A. (2008). Clathrate Hydrates of Natural Gases. New York: CRC Press.
- Smith, J. M., Van Ness, H. C., and Abbott, M. M. (2005). Introduction to chemical engineering thermodynamics. Boston: McGraw-Hill.
- Song, R., Yan, Y., Shang, L., Li, P., and Xu, J. (2020). A comparison of kinetics and thermodynamics of methane hydrate formation & dissociation in surfactant and solid dispersed emulsion. Colloids and Surfaces A: Physicochemical and Engineering Aspects, 599, 124935.
- Sum, A. K., Burruss, R. C., and Sloan, E. D. (1997). Measurement of Clathrate Hydrates via Raman Spectroscopy. The Journal of Physical Chemistry B, 101(38), 7371-7377.
- Tohidi, B., Danesh, A., Todd, A. C., Burgass, R. W., and Østergaard, K. K. (1997). Equilibrium data and thermodynamic modelling of cyclopentane and neopentane hydrates. Fluid Phase Equilibria, 138(1), 241-250.
- Veluswamy, H. P., Hong, Q. W., and Linga, P. (2016a). Morphology Study of Methane Hydrate Formation and Dissociation in the Presence of Amino Acid. Crystal Growth & Design, 16(10), 5932-5945.
- Veluswamy, H. P., Kumar, A., Kumar, R., and Linga, P. (2017). An innovative approach to enhance methane hydrate formation kinetics with leucine for energy storage application. Applied Energy, 188, 190-199.
- Veluswamy, H. P., Kumar, A., Seo, Y., Lee, J. D., and Linga, P. (2018). A review of solidified natural gas (SNG) technology for gas storage via clathrate hydrates. Applied Energy, 216, 262-285.
- Veluswamy, H. P., Kumar, S., Kumar, R., Rangsunvigit, P., and Linga, P. (2016b). Enhanced clathrate hydrate formation kinetics at near ambient temperatures and

- moderate pressures: Application to natural gas storage. Fuel, 182, 907-919.
- Veluswamy, H. P., Wong, A. J. H., Babu, P., Kumar, R., Kulprathipanja, S., Rangsunvigit, P., and Linga, P. (2016c). Rapid methane hydrate formation to develop a cost effective large scale energy storage system. Chemical Engineering Journal, 290, 161-173.
- Viriyakul, C., Jeenuang, K., Inkong, K., Kulprathipanja, S., and Rangsunvigit, P. (2021). A detailed morphology investigation on the effects of mixed anionic and nonionic surfactants on methane hydrate formation and dissociation. Journal of Natural Gas Science and Engineering, 90, 103904.
- Wang, X., French, J., Kandadai, S., and Chua, H. T. (2010). Adsorption Measurements of Methane on Activated Carbon in the Temperature Range (281 to 343) K and Pressures to 1.2 MPa. Journal of Chemical & Engineering Data, 55(8), 2700-2706.
- Xu, J., Chen, Q., and Du, J. (2020). Promotion of methane storage in tetra-n-butylammonium sulfate semi-clathrate hydrate by inducing pure methane hydrate. Chemical Engineering Journal, 127988.
- Zhang, J. S., Lee, S., and Lee, J. W. (2007). Kinetics of Methane Hydrate Formation from SDS Solution. Industrial & Engineering Chemistry Research, 46(19), 6353-6359.
- Zheng, J., Bhatnagar, K., Khurana, M., Zhang, P., Zhang, B.-Y., and Linga, P. (2018). Semiclathrate based CO<sub>2</sub> capture from fuel gas mixture at ambient temperature: Effect of concentrations of tetra-n-butylammonium fluoride (TBAF) and kinetic additives. Applied Energy, 217, 377-389.
- Zhong, Y., and Rogers, R. E. (2000). Surfactant effects on gas hydrate formation. Chemical Engineering Science, 55(19), 4175-4187.
- Harris, W. (2009). A Brief History of Methane Hydrate. Retrieved from <https://science.howstuffworks.com/environmental/green-tech/energy-production/frozen-fuel2.htm>
- Harrison, S. E. (2010). Natural Gas Hydrates. Retrieved from <http://large.stanford.edu/courses/2010/ph240/harrison1/>



## VITA

<b>NAME</b>	Siravich Junthong
<b>DATE OF BIRTH</b>	1 October 1996
<b>PLACE OF BIRTH</b>	Yala, Thailand
<b>INSTITUTIONS ATTENDED</b>	<p>2019-2021     Master of Science in Petrochemical Technology, The Petroleum and Petrochemical College, Chulalongkorn University, Bangkok, Thailand</p> <p>2015-2019     Bachelor of Science in Chemical Engineering, Department of Chemical Technology, Faculty of Science, Chulalongkorn University, Bangkok, Thailand</p>
<b>HOME ADDRESS</b>	<p>52/109 Sangchuto Rd. District/Subdistrict Tha Maka Kanchanaburi 71120, Thailand</p>
<b>PUBLICATION</b>	<p>Proceedings:</p> <p>1. Junthong, S., Yodpetch, V., Inkong, K., Kulprathipanja, S., and Rangsunvigit, P. Investigation of Methane Hydrate Formation Using a Novel Hydrate Promoter. Proceedings of The 27th PPC Symposium on Petroleum, Petrochemicals, and Polymers and The 12th Research Symposium on Petrochemical and Materials Technology, Bangkok, Thailand.</p> <p>Presentations:</p> <p>1. Junthong, S., Yodpetch, V., Inkong, K., Kulprathipanja, S., and Rangsunvigit, P. (2021). Investigation of Methane Hydrate Formation Using a Novel Hydrate Promoter. Poster Presentation at The 27th PPC Symposium on Petroleum, Petrochemicals, and Polymers and The 12th Research Symposium on Petrochemical and Materials Technology.</p> <p>2. Junthong, S., Yodpetch, V., Inkong, K., Kulprathipanja, S., and Rangsunvigit, P. (2021). Investigation of Methane Hydrate Formation Using Tetrahydrofuran and Pyrrolidine. Poster Presentation at The 30th Thai Institute of Chemical Engineering and Applied Chemistry Conference.</p>
<b>AWARD RECEIVED</b>	<p>2019     Outstanding Graduate Awards Given by Professor Dr. Tab Nilaniti Foundation, Thailand</p> <p>2019     A Full Scholarship for M.Sc. Study Given by Bangchak Corporation Public Company, Thailand</p> <p>2018     Role Model Student Awards Given by Faculty of</p>

Science, Chulalongkorn University, Thailand  
2018 Outstanding Academic Student Awards with a  
Full Scholarship Given by Faculty of Science,  
Chulalongkorn University, Thailand  
2018 Innovation Suggestion Awards Given by SCG  
Chemicals Company, Thailand



3243175980

CU ThesIs 6271006063 thesis / recv: 19072564 14:31:51 / seq: 40